Bulletin of the Geological Society of Finland, Vol. 95, 2023, pp 107–134 https://doi.org/10.17741/bgsf/95.2.002

# Secular change of tectonic setting in the Archean Takanen greenstone belt, northeastern Karelia Province, Fennoscandian Shield

VERTAISARVIOITU
KOLLEGIALT GRANSKAD
PEER-REVIEWED
www.tsv.fi/tunnus

Ville Järvinen[1,2*], Nikolaos Karampelas[2], O. Tapani Rämö[2], Tapio Halkoaho[3], Tuomo Törmänen[4], Perttu Mikkola[3] and Yann Lahaye[1]

[1]*Geological Survey of Finland, Vuorimiehentie 5, 02151 Espoo, Finland*
[2]*University of Helsinki, Department of Geosciences and Geography, Gustaf Hällströmin katu 2, 00014 Helsinki, Finland*
[3]*Geological Survey of Finland, Viestikatu 7, 70211 Kuopio, Finland*
[4]*Geological Survey of Finland, Lähteentie 2, 96101 Rovaniemi, Finland*

## Abstract

The target of this study is the Takanen greenstone belt (TGB), a small 11-km-long and east-west oriented supracrustal belt in the northern Lentua complex of the Western Karelia Subprovince (eastern Finland). We present a new geological interpretation of the TGB based on lithology, geochemistry, stratigraphy, and two new zircon U-Pb age determinations and Lu-Hf-in-zircon data.

The TGB forms a ≥800-m-thick synclinal sequence composed of intercalated mafic-komatiitic and felsic-intermediate volcanic and volcaniclastic rocks (lavas, tuffs, and tuffites ) crosscut by granitoid dykes, and metamorphosed in lower amphibolite facies with few primary volcanic textures visible. The felsic-intermediate rocks are calc-alkaline and split into strongly and weakly REE-fractionated groups. The mafic–ultramafic rocks are tholeiitic with flat REE-patterns, but some samples show LREE-enrichment. Massive Fe-sulfide layers (≤1 m) are associated with volcaniclastic rocks. Komatiites are Al-undepleted and comprise differentiated (peridotite–gabbro) and undifferentiated (dunite/serpentinite) cumulates and thin undifferentiated flows. Channel-facies komatiitic cumulates are found stratigraphically above Fe-sulfide-rich units and have potential for komatiite-hosted Ni-deposits.

Our new isotope data from two felsic-intermediate volcanic rock samples shows that the TGBs stratigraphically lowermost and uppermost units are 2.96 Ga and 2.71 Ga old, respectively. Based on Hf isotope data, the older 2.96 Ga sample contains reworked crustal material, possibly originating from ~3.2 Ga crust. In contrast, the 2.71 Ga sample is isotopically juvenile (near-chondritic), indicating an episode of juvenile crust formation in the northern Lentua Complex. No unconformity is found between the stratigraphically upper and lower parts of the TGB, but the ~250 Ma age difference (and geochemical indicators) suggests they may have formed in different tectonic settings.

The lower part of TGB stratigraphy is correlated with the ~2.94 Ga Luoma Formation in the nearby Suomussalmi greenstone belt. The 2.71 Ga volcanic unit does not have a known equivalent in greenstone belts in Finland, but a corollary is found in Russia, and a tentative correlation to a possible 2.75–2.70 Ga arc-system in Takanen–Khedozero-Bolshozero–Ilomantsi is suggested.

Keywords: Archean, greenstone belt, Takanen, Karelia province, zircon, U-Pb, Lu-Hf, stratigraphy, correlation, komatiite

*Corresponding author (email: ville.jarvinen@gtk.fi)

Editorial handling: Alexander Slabunov (email: slabunov@krc.karelia.ru)

# 1. Introduction

Archean greenstone belts are metamorphosed assemblages of volcanic and sedimentary rocks formed in various tectonic and depositional settings. They are typically found as thin curvilinear belts squeezed between (and intruded by) granitoid plutons and gneisses that dominate most Archean complexes (Thurston 2002, 2015). Archean greenstone belts bear detailed information of Archean igneous, sedimentary, and tectonic processes and are important proxies of Archean tectonics and formation of the early crust (Bleeker 2002; Slabunov et al. 2006; Hölttä et al. 2014). Single-grain zircon U-Pb and Lu-Hf isotope determinations are of prime importance in constraining the age and source of volcanic rocks in Archean greenstone belts (Andersen 2012; Lehtonen et al. 2017). Combined with lithostratigraphic characterization these methods enable stratigraphic correlation of greenstone belt sequences and may provide fundamental information Archean crustal evolution. Archean greenstone belts are also important targets for Ni and Au exploration (Thurston 2015).

The Karelia Province (Fig. 1) is characterized by Meso- to Neo-Archean greenstone belts surrounded by tonalite-trondhjemite-granodiorite (TTG) complexes. Greenstone belts in Karelia are typically highly deformed and record complex histories of mantle plume, subduction, and collision events. Most of them have been interpreted as accreted oceanic plateaus and arc-systems with either unknown, tectonic, or intrusive contacts with surrounding Archean granitoid-gneiss complex (Slabunov et al. 2006; Hölttä et al. 2014, and references therein). However, a few (Suomussalmi, Matkalahti) show some evidence for autochthonous deposition on older TTG basement (Kozhevnikov et al. 2006; Papunen et al. 2009).

This contribution brings new observations related to the topics above from the Takanen greenstone belt (TGB), which is a small 11-km-long belt in eastern Finland, dominated by supracrustal volcanic and volcaniclastic rocks ranging from komatiitic to felsic compositions (Figs. 1, 2, 3). Based on lithological association, the TGB has been considered Archean (Iljina et al. 2006), possibly representing the northern extension of the ~2.94 Ga rift-related Suomussalmi greenstone belt (Papunen et al. 2009; Karampelas 2022). We present an up-to-date review of the lithology, geochemistry, and stratigraphy of the TGB, with new zircon U-Pb ages and initial Hf isotopic compositions of two key stratigraphic units (base and top). Based on our results we suggest correlations to other Archean greenstone belts and constrain the depositional environment of the TGB. This paper stems from the unpublished M.Sc. thesis of the second author (Karampelas 2022).

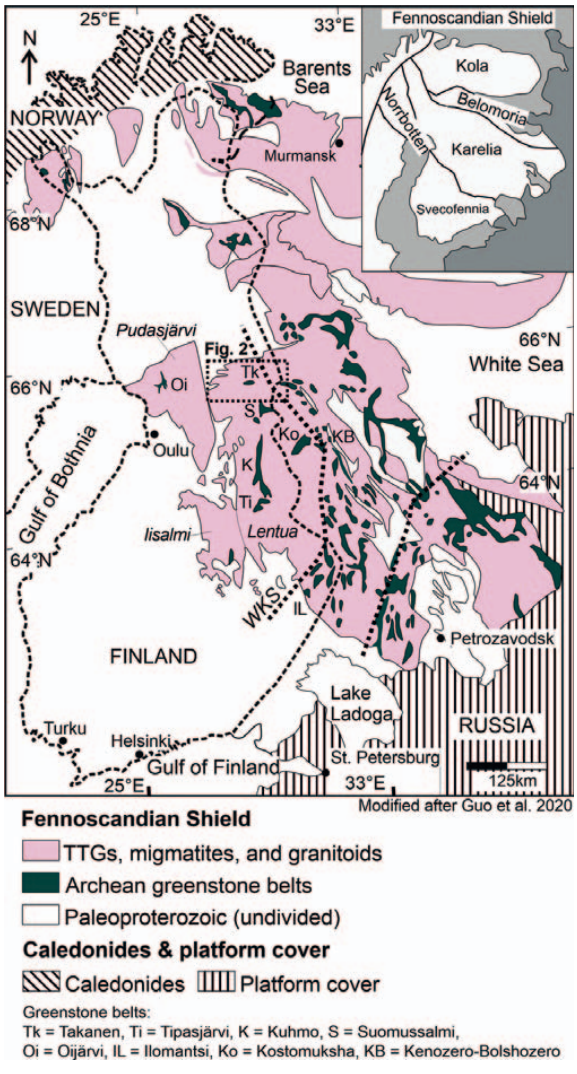


Figure 1. Simplified geological map of the northeastern Fennoscandian Shield showing the location of Archean greenstone belts (after Guo et al. 2020). Dotted line around Takanen greenstone belt (Tk) presents the extent of Fig. 2. Thick dotted lines show subprovince boundaries (WKS = Western Karelia Subprovince); Lentua, Pudasjärvi, and Ilomantsi complexes labeled (Hölttä et al. 2012b). Inset shows the geological provinces of the northeastern Fennoscandian Shield.

## 2. Geological background

The TGB is located in the Karelia Province of the Archean domain of the Fennoscandian Shield (Fig. 1). The Karelia Province is dominated by tonalite-trondhjemite-granodiorite (TTG) gneisses and greenstone belts, the latter having originated in various tectonic settings showing either arc-type, oceanic plateau, or continental rift affinities (Slabunov et al. 2006; Hölttä et al. 2014). The province is divided into three subprovinces (or terranes, *s.l.*) with distinct geological histories (Slabunov et al. 2006; Hölttä et al. 2012a). The Western Karelia Subprovince (WKS; Fig. 1) (Hölttä et al. 2012a) is a typical granite-greenstone terrane, mostly Meso- to Neoarchean in age, but locally, Paleoarchean crust exists. Based on the lithology and age of igneous suites, the WKS is further subdivided into several complexes separated by Paleoproterozoic shear zones and supracrustal belts (Hölttä et al. 2012b).

TTGs of the Lentua complex (Fig. 1) form three age groups: 2.95 Ga, 2.83–2.78 Ga, and 2.76–2.73 Ga (Vaasjoki et al. 1999; Käpyaho et al. 2006, 2007; Lauri et al. 2006; Mikkola et al. 2011; Hölttä et al. 2021). Rocks of the oldest age group are found in the northern parts of the complex in the vicinity of the Suomussalmi greenstone belt (Fig. 2). Based on inherited zircons and Sm–Nd model ages, a Paleoarchean crustal component within the northern parts of the Lentua complex has been proposed (Lauri et al. 2011; Mikkola et al. 2011; Hölttä et al. 2021). Four major Archean greenstone belts are found within the Lentua complex (Fig. 1): The Suomussalmi, Kuhmo, Tipasjärvi, and Kostomuksha belts (Hölttä et al. 2014). Of these, the oldest volcanic rocks (~2.94 Ga) have only been described from the basal Luoma Formation of the Suomussalmi belt (Huhma et al. 2012a; Lehtonen et al. 2017). Most of the volcanic rocks fall into the age groups of 2.84–2.82 Ga and 2.80–2.79 Ga (Puchtel et al. 1998; Huhma et al. 2012a; Lehtonen & Käpyaho 2016; Lehtonen et al. 2016, 2017; Slabunov et al. 2021) and are coeval with the majority of the TTG gneisses (e.g., Mikkola et al. 2011; Hölttä et al. 2021). The Suomussalmi belt shows trace-element characteristics and negative initial $\varepsilon_{Nd}$ values indicative of crustal contamination of mantle-plume sourced magmas in a continental rift setting (Papunen et al. 2009; Huhma et al. 2012a,

b; Lehtonen et al. 2017). In contrast, the Kuhmo, Tipasjärvi and Koshtamuksha belts all show juvenile or depleted mantle isotopic compositions and have been interpreted as accreted oceanic plateaus (Puchtel et al. 1998; Kozhevnikov et al. 2006; Huhma et al. 2012b; Maier et al 2013; Hölttä et al. 2014).

The Ilomantsi greenstone belt located in the Central Karelia Subprovince (Fig. 1) is, compared to the greenstone belts of the Lentua complex, distinctly younger as the majority of the volcanic units are aged 2.75 Ga (Vaasjoki et al. 1993; Huhma et al. 2012a). Similar results have been obtained from the Khedozero-Bolshozero belt (Fig. 1) with volcanic rocks providing ages between 2.71–2.70 Ga (Myskova et al. 2020). Both belts are dominated by metasediments and felsic volcanic rocks with arc signatures and have been considered as continental margin subduction systems (Sorjonen-Ward 1993; Hölttä et al. 2014; Myskova et al. 2020).

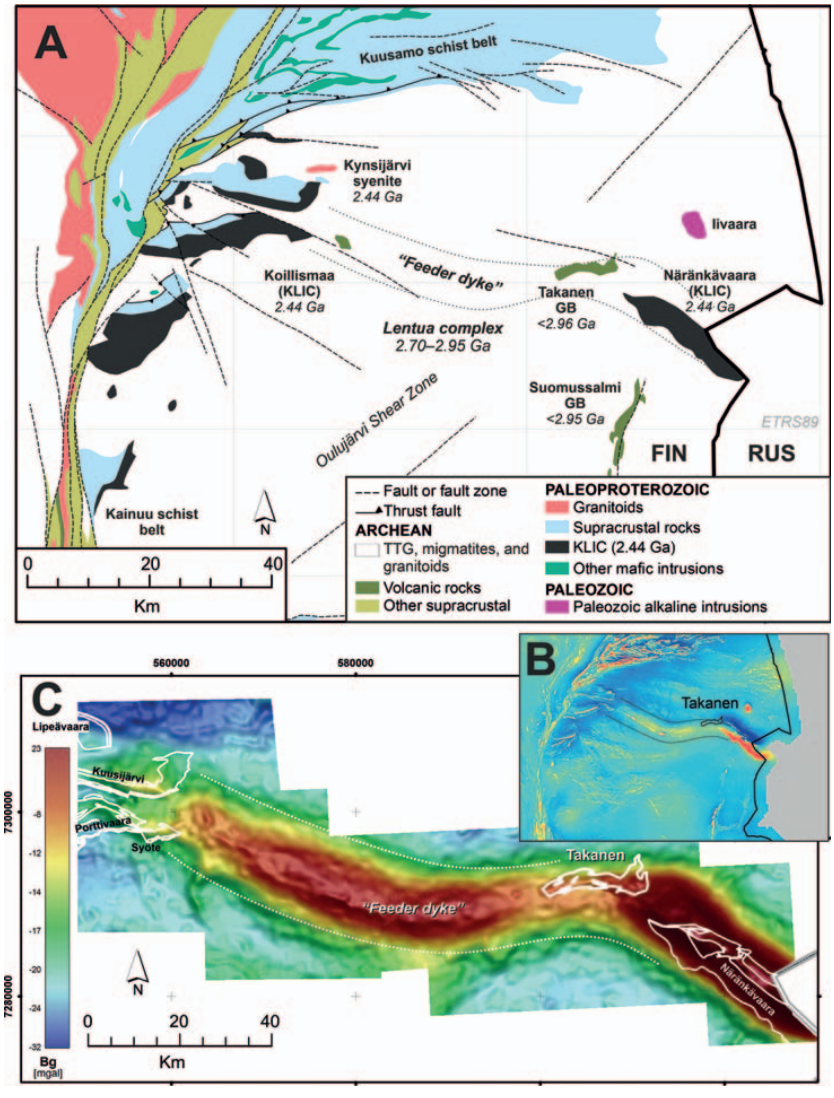


Figure 2. a) Simplified lithological map of the northern Lentua complex (Bedrock of Finland – DigiKP). b) Total magnetic intensity map illustrating the positive magnetic anomaly (dotted black outline) connecting the 2.44 Ga mafic-ultramafic Koillismaa and Näränkävaara layered intrusions (Alapieti 1982; Karinen 2010; Järvinen 2022). c) Bouguer anomaly map illustrating the location of the Takanen greenstone belt partly on top of the "feeder dyke" anomaly (dotted white outline; Takanen and the 2.44 Ga intrusions outlined in white); Figure c by H. Salmirinne.

Overall, the depositional basement of the Karelian greenstone belts is not clear (Hölttä et al. 2014). In many cases the volcanic rocks are older than the surrounding TTG (e.g., Kuhmo, Koshtomuksha) or the contact with surrounding rocks is intrusive or tectonic; no unconformities have been identified. The ~2.94 Ga Luoma Formation of the Suomussalmi belt (Fig. 1) may have been deposited autochthonously on >3.0 Ga TTG substrate (Martin et al. 1984; Luukkonen 1992; Papunen et al. 2009; Lehtonen et al. 2017).

Based on age and composition, granitoids of the WKS can be divided into four groups: 1) TTGs, 2) sanukitoids, 3) quartz diorite–quartz monzodiorite (QQ), and 4) granodiorite-granite-monzogranite (GGM) (Käpyaho et al. 2006; Mikkola et al. 2011). Plutonic activity was dominated by TTGs until 2.75 Ga; that is, during and after the cessation of volcanic activity in the Lentua complex at 2.79 Ga. A limited number of TTGs yield ages down to 2.72–2.71 Ga (Mikkola et al. 2011, 2012). TTG magmatism was followed by the ~2.72 Ga granitoids of the sanukitoid suite (Heilimo et al. 2010), originating from a lithospheric mantle enriched in LILE during subduction. Sanukitoids were in turn followed by the ~2.70 Ga QQ intrusions from a less enriched and isotopically more juvenile source (Mänttäri & Hölttä 2002; Mikkola et al. 2012). The last voluminous magmatic event in the WKS was the emplacement of 2.7 Ga anatectic leucogranitoids (GGM) as small intrusions and dykes. The GGM are coeval with the main migmatisation event of the TTG gneisses (Käpyaho et al. 2006, 2007; Mikkola et al. 2011, 2012). Overall, the varying histories of the individual subprovinces and complexes within the Karelia Province reflect complex tectonic–magmatic processes of Archean crustal formation and accretion preceding the final amalgamation of the continent corresponding to the present Karelia Province at about 2.7 Ga (Lauri et al. 2011; Hölttä et al. 2012a, 2014, 2021).

# 3. Earlier work in the Takanen greenstone belt

The Takanen greenstone belt is 11 km long and 2–3 km wide (Figs. 2a, 3a). The belt is completely covered by glacial deposits and the eponymous lake Takanen. The Paleoproterozoic Kuusamo schist belt is located 30 km to the north and the Archean Suomussalmi greenstone belt 15 km to the south (Fig. 2a). The TGB neighbors the 2.44 Ga mafic-ultramafic Näränkävaara intrusion (Fig. 2) (Alapieti 1982; Järvinen 2022), which together with the tectonically fragmented Koillismaa intrusion further west, and a large-scale linear positive magnetic and gravity anomaly ("feeder dyke") that connects the two intrusions, forms the Koillismaa–Näränkävaara layered igneous complex (KLIC) (Alapieti 1982; Karinen 2010). The TGB is located on top of the feeder dyke anomaly (Fig. 2c). It has been hypothesized that the anomaly represents a long-lived trans-crustal structure and a pathway for mantle-sourced magmas both in the Archean (TGB) and Proterozoic (KLIC) (e.g., Järvinen 2022; Karampelas 2022).

Sporadic mineral exploration has been conducted in the TGB since the late 1980's (Fig. 3a) (Vanhanen 1990; Iljina 2003; Vesanto 2003). Based on drill core observations, the belt consists of interlayered komatiites and mafic to felsic schists and gneisses interpreted as volcanogenic. Magnetic anomalies are associated with komatiitic cumulates (Fig. 3a), and conductivity anomalies with stratiform barren Fe-sulfide layers (<1 m thick) continuous along strike and associated with both felsic and mafic volcaniclastic rocks. No mineral deposits have yet been found (see Rasilainen et al. 2012).

The belt is surrounded by Archean TTG rocks. In 2003, the Geological Survey of Finland (GTK) probed the "feeder dyke" anomaly by drilling a 1.2-km-deep drill hole collared in the TGB (R339 in Fig. 3e) (Iljina et al. 2006). Notably, the hole intersects the contact between the lowermost ~500 m of the TGB (felsic volcanic rock) and the underlying Archean TTG rocks, as described later.

# 4. Methods & Materials

## *4.1 Whole-rock samples*

All of our petrographic observations are based on drill core logging and samples derived from them. A total of 32 drill holes, mostly 50–150 m in length, have been drilled into the TGB (Fig. 3). All whole-rock geochemical samples used in this study come from previous projects (Vanhanen 1990; Iljina 2003; Vesanto 2003; Iljina et al. 2006). Results include 202 X-ray fluorescence (XRF), 154 inductively coupled mass spectrometry (ICP-MS), and 362 precious metal (Au, Pd, Pt) whole-rock analyses. Note that the deepest drill hole (R339) has been extensively sampled which may cause some bias in the dataset (42 of the 202 XRF analyses are from R339). In addition to the drill core samples, analyses of 48 "top-of-bedrock" samples taken during basal till sampling are included in the geochemical data set (Fig. 3a; Iljina 2003). Petrography has been determined with polarized-light microscopy from 223 thin sections.

Whole-rock analyses were performed at the Geological Survey of Finland geochemical laboratories. Analysis method codes (in parentheses) are described in Rasilainen et al. (2007). Major elements and some trace elements were analyzed by XRF from pressed powder pellets (method 175X). The rare-earth elements (REE) and selected trace elements were analyzed by ICP-MS after total dissolution (methods 308M/P). Precious metals (Au, Pd, Pt) were analyzed by graphite furnace atomic absorption spectrometry (GFAAS) after preparation by either Pb fire-assay (methods 704/705U) or Hg-precipitation (methods 519/521U). Detection limits for REE are 0.1–0.5 ppm and for precious metals 1–10 ppb. The analytical data are attached as an Electronic Appendix (attachment S1). Whole-rock geochemical results have been normalized to volatile-free 100 wt.%, and Mg# has been calculated as molar $Mg/(Mg+Fe_{tot})$.

## *4.2 U-Pb and Lu-Hf isotope analyses*

### 4.2.1 Sample selection and preparation

Three whole-rock samples comprising 2–3 m of halved drill core were collected for zircon separation and isotope analysis (samples A2609, A2610, and A2611 in Table 1). Sampling locations are marked with stars in Fig. 3b and 3e. Separation of sample A2609 did not produce zircon and it is dismissed.

Zircon grains for U-Pb dating were selected by hand-picking after crushing and milling, heavy liquid and magnetic separation. Zircons were mounted in epoxy resin, sectioned approximately in half, and polished. Back-scattered electron (BSE) and cathodoluminescence (CL) images were used to target the analysis spots.

### 4.2.2 U-Pb LA-ICPMS analyses

Single-grain zircon U-Pb dating analyses were performed at the Geological Survey of Finland in Espoo by using a Nu Plasma AttoM single collector LA-ICP-MS connected to a Photon Machine Excite laser ablation system. Detailed description of the applied method can be found in Molnár et al. (2018) and is also attached in Appendix S1. Calibration standard GJ-1 (609 ± 1 Ma; Belousova et al. 2006) and in-house standards A382 (1877 ± 2 Ma) and A1772 (2711 ± 1 Ma; Huhma et al. 2012a) were run at the beginning and end of each analytical session, and at regular intervals during sessions. Plotting of the U-Pb isotopic data and age calculations were performed using the Isoplot/Ex 4.15 program (Ludwig 2003). All ages were calculated with 2σ errors and without decay constants errors. All errors in the figures are at the 2σ level.

### 4.2.3 Lu-Hf LA-ICPMS analyses

Single-grain zircon Lu-Hf isotope analyses were performed at the Geological Survey of Finland in Espoo by using a Nu Plasma HR multi-collector ICP-MS and a Photon Machine Analyte G2 laser

Table 1. Characteristics of whole-rock samples taken for zircon separation and properties of obtained separates.

| Name | Drill hole interval | Stratigraphy and lithology | Petrography | Zircon morphology | Zr in whole-rock | Age (±2sd) |
|---|---|---|---|---|---|---|
| A2609 | M452398R318 23.90–26.90 m | Stratigraphically from the lower-half of the belt; from a 5 m-thick intermediate–felsic volcano-sedimentary interlayer between units of tholeiitic basalt | Foliated fine grained greenstone assemblage (Pl-Qz-Am-Bt), no primary textures identified | No zircons obtained | 191 ppm | na |
| A2610 | M452398R332 61.5–63.60 m | From the upper part of TGB stratigraphy (center of the syncline depicted in Fig. 3b). Felsic-intermediate volcanic interlayer between a komatiitic basalt (below) and a tholeiitic basalt (above) | Fine-grained (< 1mm) feldspar-quartz-biotite schist with cm-scale compositional layering, weakly grano-/lepidoblastic, locally quartz/felspar clasts (after volcanic material?); protolith could be a tuff or redeposited volcanic material | About 70 zircons were recovered.<br><br>In CL images (not shown) grains show euhedral prismatic habits with crystal faces, but grains are commonly fractured giving them an anhedral appearance in BSE images (Fig. 9a-b).<br><br>Grain size varies between 50–150 µm, and length/width ratios between 1.1–2.4. Grains are unzoned or very weakly zoned in BSE images. | 217 ppm | 2706 ± 4 Ma |
| A2611 | M452398R339 276.90–278.70 m | From the lowermost unit of TGB stratigraphy (Fig. 3e). Near the top of a 250–500-m-thick felsic volcanic unit, in sharp contact with a tholeiitic basalt unit above, and texturally gradational contact to Archean TTG rocks below (see text). | Quartz-feldspar-mica schist characterized by relatively angular clasts of quartz (2–3 mm) and feldspar (<10 mm); protolith could be a tuff or redeposited volcanic material | About 110 zircons were recovered.<br><br>In CL images (not shown) grains show euhedral prismatic habits. All grains show oscillatory zoning in BSE images, and some grains contain relict cores. Some grains also show unzoned rims (Fig. 9c-d). Most grains contain some metamict parts, typically towards the rims.<br><br>Grain size varies between 50–250 µm, and length/width ratios between 1.4–5.9; some grains are strongly elongated. | 118 ppm | 2958 ± 8 Ma |

microprobe over or adjacent to the U-Pb analysis spots. Detailed description of the applied method can be found in Heilimo et al. (2023) and is also attached in Appendix S1. For the calculation of $\varepsilon_{Hf}$ values we used present-day chondritic $^{176}Hf/^{177}Hf$ = 0.282785 and $^{176}Lu/^{177}Hf$=0.0336 (Bouvier et al. 2008). The standard/reference zircon GJ-1 was run as unknown at frequent intervals. The observed external reproducibility on the GJ-1 reference zircon gives a 2σ-uncertainty estimate of ± 1.6 ε-units on single spot analysis.

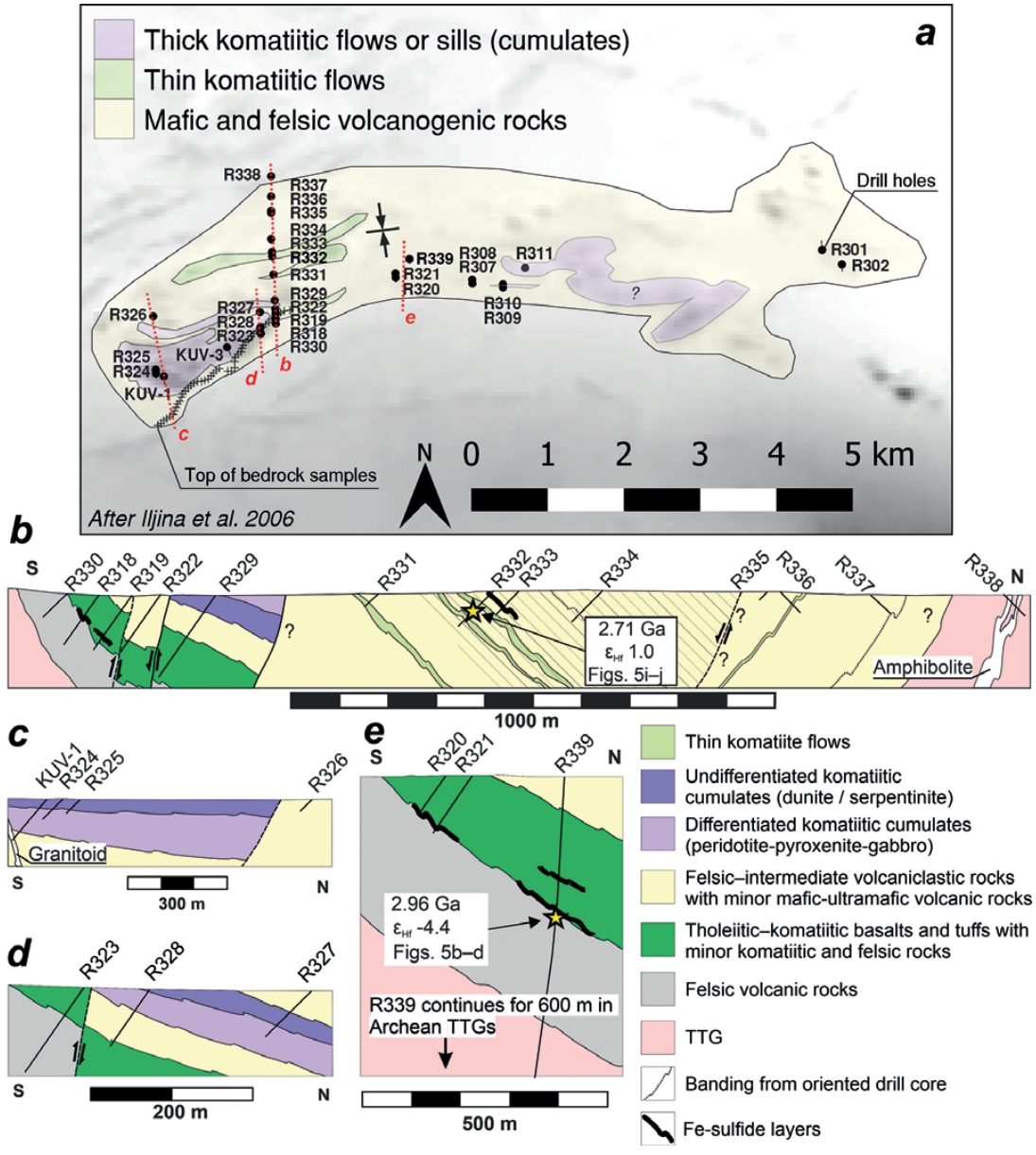


Figure 3. a) Simplified geological map of the Takanen greenstone belt (Bedrock of Finland – DigiKP) on aeromagnetic map (black = high total magnetic intensity). b)–e) Simplified cross-sections (marked with red dotted lines in *a*). The belt is interpreted as a syncline with youngest units in the center (hatched area in *b*). Zircon sampling locations are marked with stars with labels showing summary results.

# 5. Results

## 5.1 Lithology and stratigraphy of the Takanen greenstone belt

Lithology and stratigraphy of the belt is summarized in Fig. 3. The Archean TTGs underneath the southern contact are strongly foliated and folded heterogeneous grey biotite tonalite gneisses (Fig. 5a) crosscut by several granitoid dykes (GGM?) and locally migmatized (Iljina et al. 2006). The TGB is mostly composed of fine grained (meta) volcanic and volcaniclastic schists and gneisses metamorphosed at lower (epidote)-amphibolite facies. Due to rarity of the preserved primary textures, the rocks have been classified based on their whole-rock composition into two suites (see next section). First, a mafic-ultramafic tholeiitic suite composed of komatiites and komatiitic-tholeiitic basalts, and second, a felsic-intermediate calc-alkaline suite composed of volcaniclastic rocks.

The structure of the belt is poorly constrained but based on unit correlations and oriented drill core samples (n=6) we interpreted it as a syncline, with the southern limb dipping 45–75° north and the northern limb dipping ~75° south (Fig. 3b). The stratigraphic sequence of the TGB is estimated to be at least 800 m thick. Based on the age data (this study), the TGB consists of stratigraphically lower part (<2.96 Ga, most of the belt) and an upper part in the center of the syncline (~2.70 Ga, hatched section in Fig. 3b). Lithologically, both parts are similar, being composed of interlayered sequences of the aforementioned rock types. Proportions and occurrence styles of komatiitic and tholeiitic rocks differ, however, with thick continuous sequences restricted to the lower part of the belt (Fig. 3).

***Stratigraphically lower part (<2.96 Ga)***

The lowermost unit of the TGB is intersected along the southern border of the TGB (Fig. 3b and 3e). It consists of strongly foliated plagioclase-quartz-biotite gneiss, locally with plagioclase porphyroclasts and phenocrysts (Figs. 5b–d), and is homogeneous compared to the underlying TTGs (Fig. 5a). We interpreted this unit as a felsic volcanic rock. No exact lithological contact, unconformity, or fault was observed in drill core. Instead, there is a textural gradation from the strongly gneissose heterogeneous TTGs (e.g., cm-scale augen) to the weakly gneissose and homogeneous felsic volcanic rock of the TGB. A change to more homogeneous geochemical and petrophysical characteristics can be seen in drill hole R339 at a depth of 495 m (Fig. 4). We concur with Iljina et al. (2006) and interpret this as the basal contact of the TGB.

One-meter-thick semi-massive Fe-sulfide layer is found at the upper contact of the basal felsic volcanic unit (Fig. 3e, 4). This is followed by a 200 m interval of tholeiitic- and minor komatiitic basalt (Fig. 3e). The basalts are composed of amphibole, plagioclase, biotite, and minor epidote (Fig. 5e); komatiitic basalts are richer in amphibole. In drill core, the rocks are dark green to grey, foliated, and range from coherent homogeneous 5–100 m intervals to banded on the cm-dm scale. Homogeneous basalts are clearly lavas; thin quartz-feldspar veinlets are common, and few brecciated sections with similar white infill may represent inter-pillow material but no obvious pillow structures were observed. Compositional banding may indicate volcaniclastic tuffs/tuffites or thin flows (Figs. 5f, g). The basalt sequence is followed by a unit of intermediate volcanic rocks which have the same mineral assemblage as the basalts but are richer in biotite and also contain quartz. Correlations between profiles in Fig. 3b and 3e are not exact, and from this point upwards stratigraphy of the belt is less well constrained.

Above the basalt-rich section, the stratigraphy of the belt is dominated by fine-grained felsic-intermediate plagioclase-quartz-biotite schists and gneisses intercalated with 1–20 m thick units of mafic-ultramafic lavas and tuffs. Contacts are sharp or diffuse and no major tectonic contacts or unconformities are identified. The felsic-intermediate schists are grey, foliated, and sometimes complexly folded, and either homogeneous or thinly banded on the cm-scale. Possible pyroclastic types contain aggerate

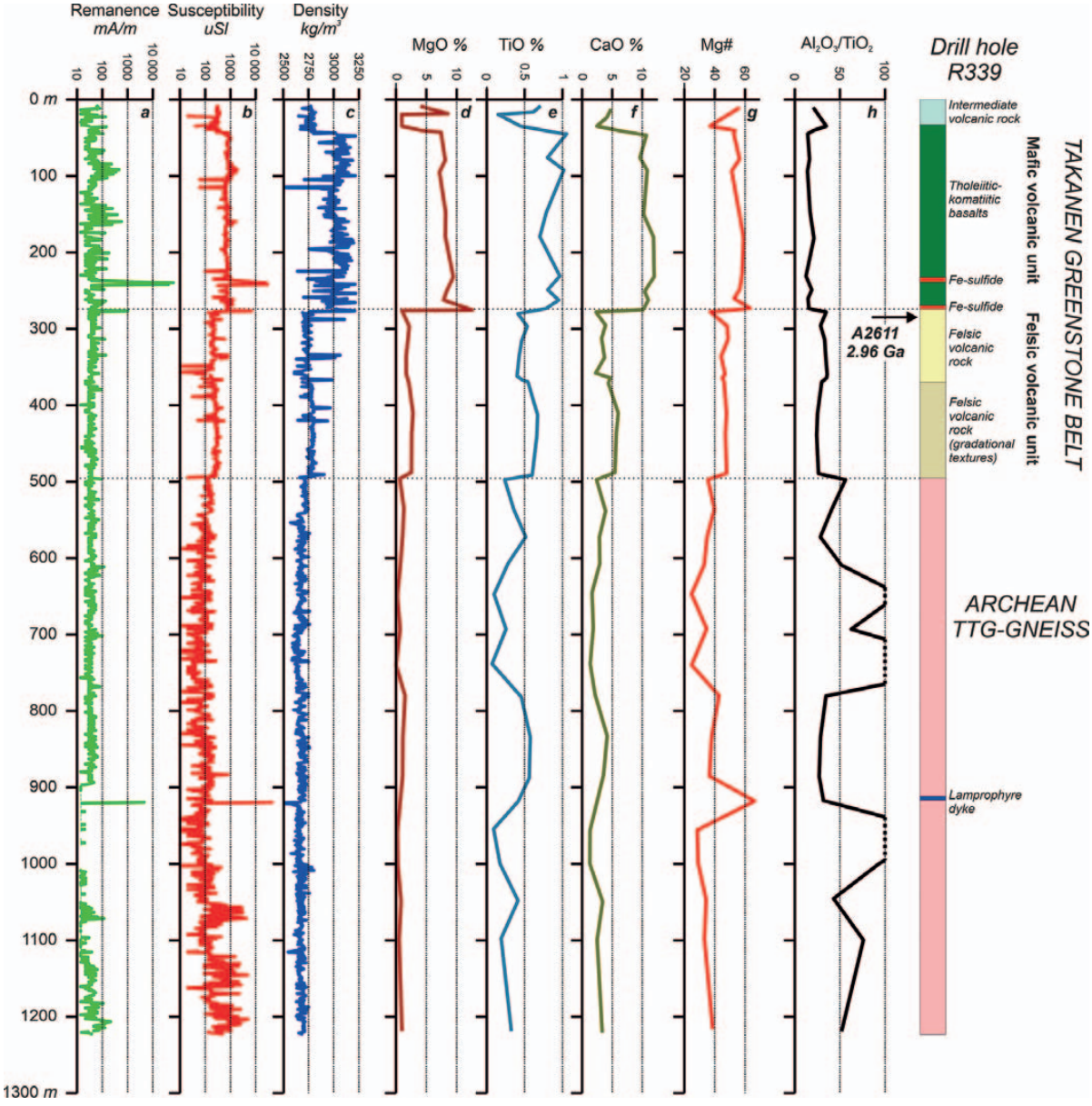


Figure 4. Drill core log of hole R339 (see Fig. 3e), with petrophysical (a–c), whole-rock geochemical (d–g) and lithological data plotted (modified from Iljina et al. 2006). Contact between the underlying heterogeneous Archean TTG rocks and the homogeneous basal 2.96 Ga felsic volcanic unit of the Takanen greenstone belt is located at ~495 m.

plagioclase-quartz clasts up to 3–10 mm size (Fig. 5i). Banded finer grained schists show shear bands but also locally suggest relict bedding or lamina (Fig. 5g). Strongly deformed types show gneissose fabrics (Fig. 5h). Textural variation in the felsic-intermediate schists probably reflects both primary depositional features and strain partitioning during deformation.

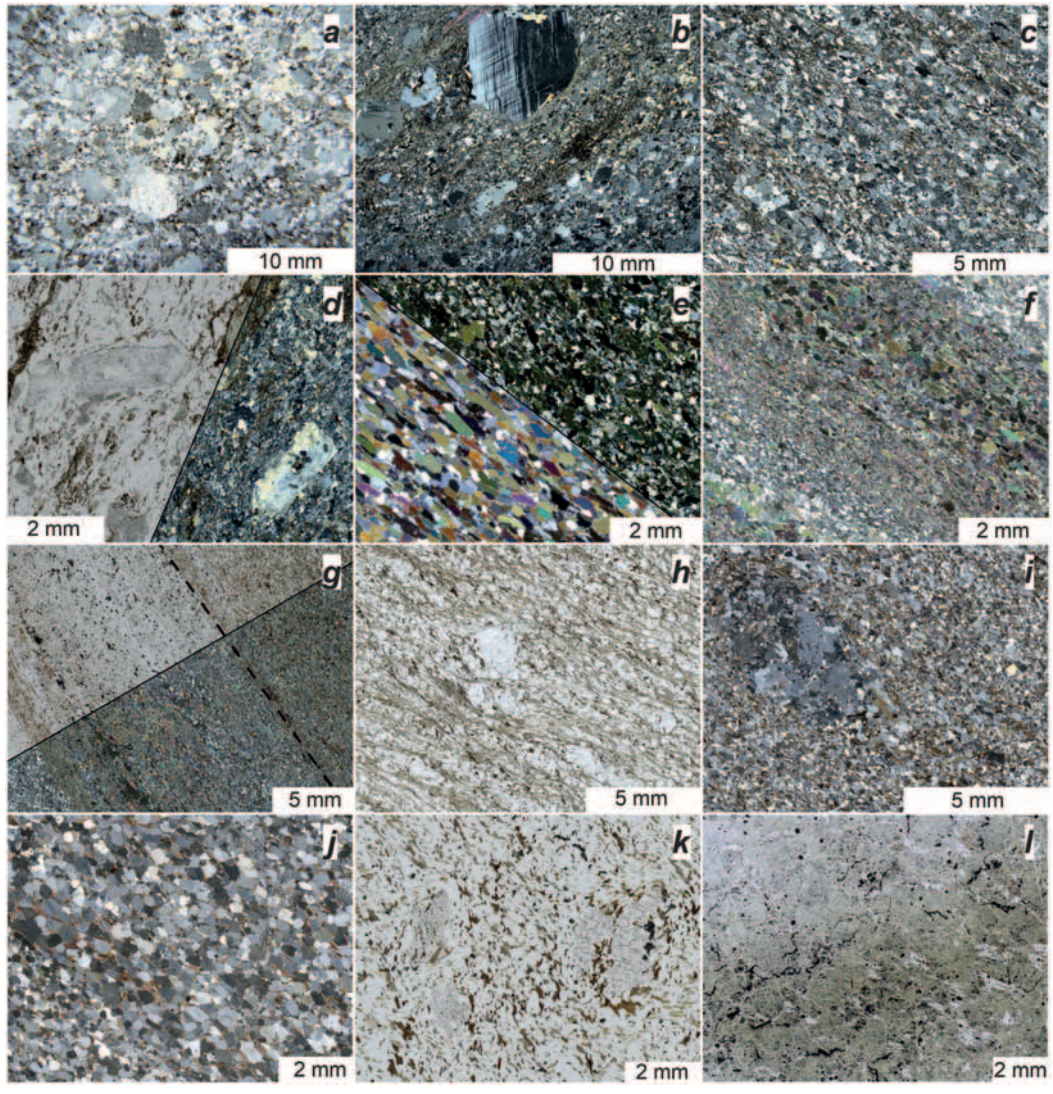


Figure 5. Photomicrographs photos of main rock types in the Takanen greenstone belt (TGB). In parentheses, drill hole id and sample depth; parallel-polarized = PP, Cross-polarized = XP. Abbreviated mineral names are quartz (Qz), plagioclase (Pl), biotite (Bt), amphibole (Am), epidote (Epi). a) Archean TTGs in drill hole R339 are strongly foliated and folded heterogeneous tonalitic gneisses with 1–5 cm Qz-Pl lenses and 0.5–2 cm fragments surrounded by Bt-rich seams (sample R339 689.60 m, XP). Lowermost felsic volcanic unit (b–d): b) fine to mid grained Pl-Qz-Bt gneiss with up to 10 mm plagioclase porphyroclasts (secondary muscovite in fractures); U-Pb dating sample A2611 (2.96 Ga) from this interval (R339 277.75 m, XP). c) homogeneous Pl-Qz-Bt gneiss (R318 79.9 m, XP). d) Pl-Qz-Bt gneiss with sericited Pl porphyroblasts or relict phenocrysts (R323 50.40 m, left PP, right XP). e) Lower-left is typical homogeneous tholeiitic (meta)basalt with assemblage Am-Pl-(Bt-Epi) (R318 35.20 m, XP). Upper-right is LREE-enriched basalt with same assemblage (R321 123.35m, XP). f) Thin komatiitic flow (20 wt.% MgO) with banded texture showing alternating Am and Am-Pl-rich layers (R319 89.30 m, XP). g) Thinly intercalated mafic-felsic schists with mm–cm scale compositional layering (primary bedding in tuffites?). Dashed line separates alternating Pl-Bt-Qz and Am-Pl-(Bt-Qz) -rich layers (R319 108.10 m, upper-left PP, lower-left XP). h) Sheared Pl-Qz-Bt gneiss (R322 28.30 m, PP). Felsic-intermediate volcanic/volcaniclastic rocks of the uppermost part of TGB stratigraphy (i–j): i) Pl-Qz-Bt schist showing a 5 mm Pl-Qz-Bt clast (possible relict pyroclast?) (R332 98.40 m, XP). j) weakly banded lepidoblastic Pl-Qz-Bt schist; U-Pb dating sample A2610 (2.71 Ga) from this interval (R332 39.50 m, XP). k) Grano-/lepidoblastic Pl-Qz-Bt gneiss with sieve-textured garnet porphyroblasts (R326 21.00 m, PP). l) Serpentinite with relict olivine-(chromite) adcumulate texture, secondary magnetite on grain boundaries (R325 30.95 m, PP).

***Komatiites***

Komatiites are found as thin flows and thick cumulate bodies. The komatiitic interlayers within the lowermost basalt sequence (Fig. 3b) appear as relatively thin (<5 m; Fig. 5f) discontinuous lenses as they are not intersected in all drill holes (e.g., in R339). Magnetic anomalies are commonly associated with thick (at least 20–50 m) homogeneous serpentinite bodies, interpreted as komatiitic lava channel cumulates (Fig. 3a). In the western end of the belt, better preserved komatiitic cumulates are found and two flow-units can be identified (Figs. 3c, d). The lower unit is a 60–80 m thick upwards-fractionated cumulate series composed of harzburgite, olivine pyroxenite, and gabbro. It likely represents a ponded flow or a sill. The upper flow-unit is a 20-m-thick undifferentiated dunite (channel facies olivine adcumulate) with a sharp contact to the underlying pyroxenite. The dunite contains pseudomorphs after olivine and trace amounts of disseminated cumulus chromite (Fig. 5l). Dip of both units is shallow and becomes subhorizontal in the western end of the belt (Fig. 3c). Footwall rocks of these cumulate bodies vary from basalt to felsic volcaniclastic rocks, and both sharp and hybridized (partly molten) contacts are observed suggesting an upwards younging direction.

***Stratigraphically uppermost part (2.71 Ga)***

Towards the north and northwest textures become lepidoblastic and equigranular (0.1–1 mm) (Fig. 5j); some drill holes also contain garnet porphyroblasts (Fig. 5k). More equilibrated lepidoblastic textures and garnet imply an increasing metamorphic gradient towards the north (garnet in R326 and R332–334 in Fig. 3a). The stratigraphically uppermost part of the TGB (cross-hatched section in Fig. 3b) is composed of fine grained weakly layered lepidoblastic plagioclase-biotite-quartz schists of andesitic-dacitic composition, locally with possible relict pyroclasts (Figs. 5i, j), and with 0.5–5 m interlayers of basalt and komatiite. A felsic-intermediate layer bounded by mafic units above and below is interpreted as pyroclastic and was sampled for zircon U-Pb dating (sample A2610 in Table 1; Fig. 5j). Although lithologically similar to the underlying stratigraphy, this uppermost felsic-intermediate unit has a very distinct trace-element and isotopic composition (next sections).

***Sulfide layers***

Several massive to semi-massive Fe-sulfide layers are found in the TGB. Three thickest layers are 0.5–1 m thick (Figs. 3b, e) with several thinner layers also found. The layers are associated with felsic and less often mafic volcaniclastic rocks, typically at unit contacts but also within units. The lowermost sulfide layer is found along the contact between the lowermost felsic and mafic volcanic units (Figs. 3b, e). The irregular layers are composed of compact pyrrhotite and minor pyrite with trace chalcopyrite, and with abundant felsic lithic clasts (breccia?) supported by sulfide matrix, such that the total sulfide volume is about 30–60 vol.%. In the eastern end of the belt, pegmatitic granites crosscut supracrustal rocks of the TGB, with massive hydrothermal (or remobilized?) sulfide veins cutting and brecciating other rock types (Vanhanen 1990). Disseminated sulfides are also found in all rock types in Takanen typically in minor amounts, but can locally be up to 1 wt.% S. All sulfide occurrences regardless of texture and host rock association are metal-poor except for Fe (Vanhanen 1990; Iljina et al. 2006).

***Dykes***

In addition to supracrustal rocks, the TGB is crosscut by locally abundant and generally 1–10 m thick granitoid dykes (see Vanhanen 1990). Three types are observed:

1) Dark colored fine-grained feldspar-phyric (1–3 mm) granodiorites typically forming thin (<1 m) and undeformed dykes;
2) Pale medium grained feldspar-phyric (2–5 mm) granite-granodiorites typically forming 1–2-meter-thick weakly deformed dykes; and
3) White or reddish quartz-rich granite pegmatites.

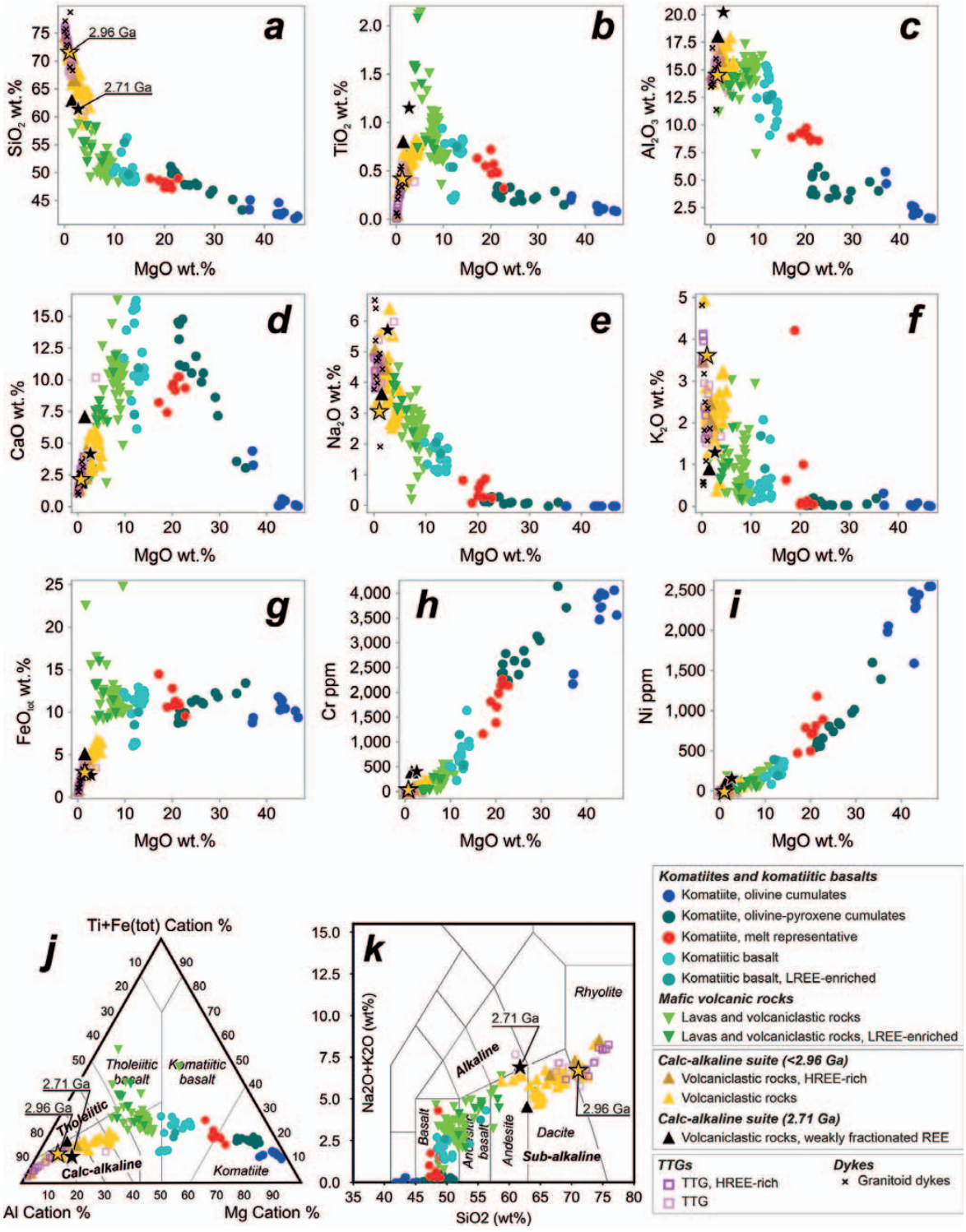


Figure 6. Whole-rock geochemical compositions of samples from the Takanen belt on variation diagrams. a–i) MgO on the X-axis vs. $SiO_2$, $TiO_2$, $Al_2O_3$, CaO, $Na_2O$, $K_2O$, $FeO_{tot}$ and Ni, and Cr on the Y-axis. j) Jensen cation diagram, k) TAS diagram. Age determination samples marked with yellow (A2611) and black (A2610) stars. Note that most other geochemical diagrams in this paper use the same colors/symbols.

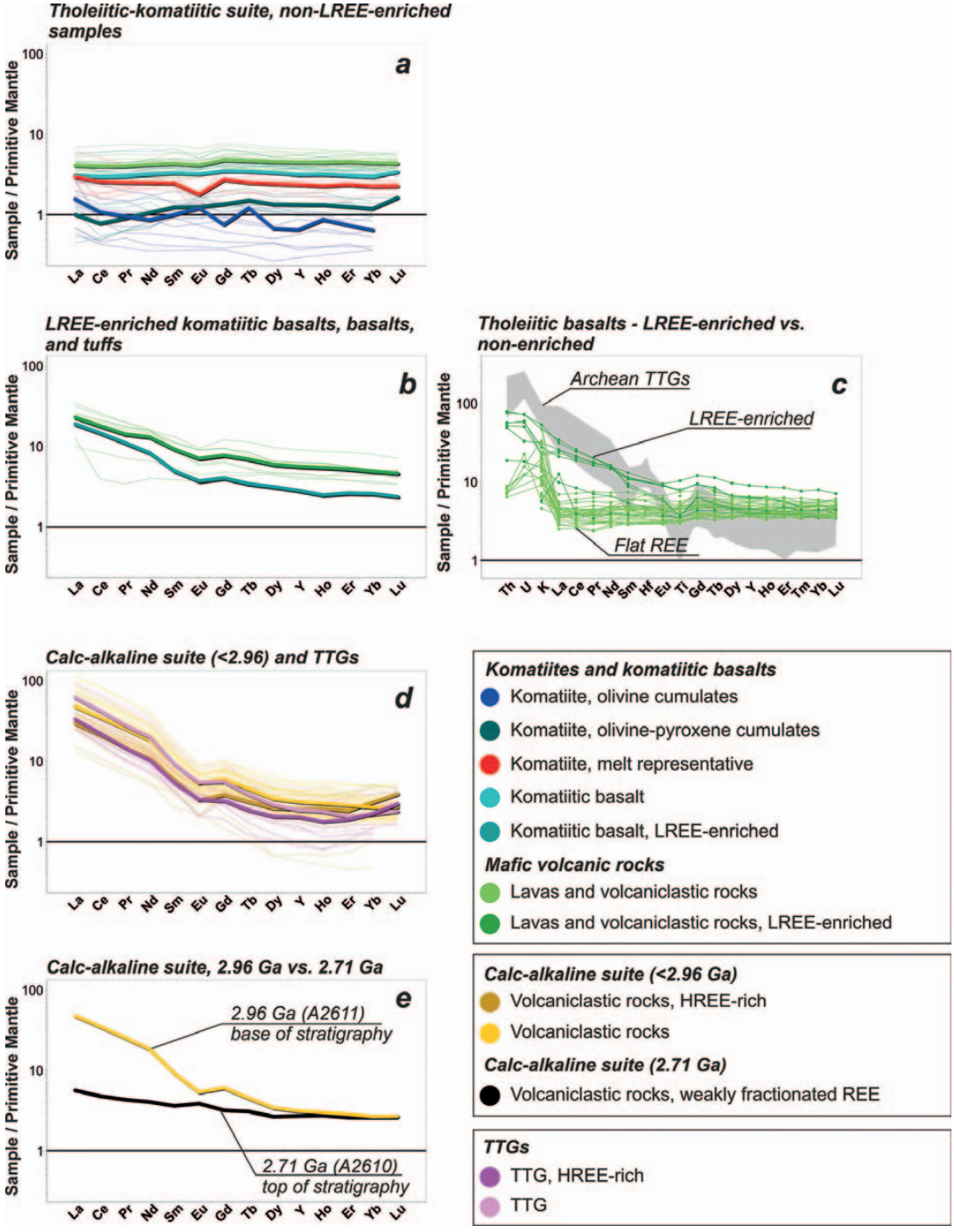


Figure 7. Trace element patterns of whole-rock samples from the Takanen greenstone belt (a–e) normalized to primitive mantle (McDonough & Sun 1995). Thick lines indicate group averages (same groupings as in Fig. 6) and thin lines indicate individual samples. c) Comparison between LREE-enriched and non-enriched tholeiitic basalts illustrating possible crustal contamination signature (TTG samples from drill hole R339 grouped and plotted in grey). d) Note subdivision to slightly HREE-enriched and non-enriched groups found both in the older volcaniclastic suite and in the TTG samples. e) REE-patterns of two felsic-intermediate volcanic rocks dated in this study (Table 1); note very weak REE-fractionation of the younger 2.71 Ga calc-alkaline suite (n=2).

The granitoid dykes have not been dated, but at least some likely represent the ~2.7 Ga GGM magmatism (Käpyaho et al. 2006; Lauri et al. 2006). Few diabase dykes are found and are assumed to be Proterozoic. Few lamproite and lamprophyre dykes are found crosscutting the TTG's and the lowermost part of the TGB (Iljina et al. 2006).

## 5.2 Geochemistry

Whole-rock geochemical variations in the Takanen greenstone belt are illustrated in Figs. 6 and 7. Samples have a bi-modal distribution (Fig. 6j), consisting of a komatiitic-tholeiitic mafic-ultramafic suite and a calc-alkaline felsic-intermediate suite.

***Calc-alkaline suite and TTGs***

Felsic-intermediate volcaniclastic rocks making up the calc-alkaline suite are, based on their major element compositions, sub-alkaline andesites-dacites-rhyolites (Figs. 6j, k). Primary division of the calc-alkaline suite into two groups is based on the distinct REE patterns between the two groups (Fig. 7e).

The older, lower group (n=31) encompasses the southern and northern parts of the belt (Fig. 3b), and shows strongly LREE-enriched trace element patterns with Eu/Eu* of 0.6–1.0 (Figs. 7d, e). Samples of the lower group are geochemically similar to the Archean TTGs (Fig. 6). Both are LREE-enriched, with similar flat-HREE and slightly HREE-enriched subgroups (Fig. 7d). The older volcaniclastic and TTG samples show average values for $(La/Yb)_N$ of 16 and 24 and for Sr/Y of 26 and 32, respectively. These are transitional values between the Archean TTG and calc-alkaline magma series as defined by Condie (2014).

The younger, uppermost group (n=2), present only in the center of the syncline (cross-hatched in Fig. 3b), plots as andesite-dacite in Fig. 6k and shows higher contents of Ni (140 ppm) and Cr (420 ppm) compared to the calc-alkaline samples of the lower group (40 ppm Ni and 80 ppm Cr). The younger group (n= 2) shows very weakly fractionated REE-patterns with average $(La/Yb)_N$ of 2, Eu/Eu* of 1.1–1.2, and total REE abundances similar to tholeiitic samples (Figs. 7e, 8). Average Sr/Y is 14. These values suggest island arc or plateau affinity (Condie 2014).

***Mafic-ultramafic rocks***

The mafic-ultramafic rocks show flat or weakly LREE-depleted patterns with REE-abundances approximately 1–5 times relative to primitive mantle (PM, Fig. 7a). Tholeiitic basalts (Fig. 7c) have 0.5–1 times REE-abundance (n=30) of MORB (not shown). They show positive anomalies for the fluid-mobile elements Rb, Ba, K, Sr, and weak negative anomalies (Eu/Eu*=0.75–1.05). An exception is a group of tholeiitic-komatiitic basalt samples with LREE-enriched patterns (n=11) and positive Rb, Ba, K, Sr, Th, U anomalies suggesting crustal contamination (Fig. 7b).

Komatiites are characterized by high MgO (>18 wt.%), Ni (500–2500 ppm) and Cr (1200–4000 ppm) (Fig. 6). They plot as Al-undepleted komatiites in Fig. 8. Thicker serpentinite bodies contain 40–46 wt.% MgO and fall on olivine control lines in various diagrams (not shown) indicating the rocks are almost pure olivine cumulates. MgO-poorer cumulates (20–35 wt.% MgO) plot between olivine-pyroxene control lines suggesting that they represent olivine-clinopyroxene cumulates, also corroborated by relatively high CaO contents of these samples (Fig. 6d). Komatiitic basalts contain less $Al_2O_3$ and more MgO and Cr compared to tholeiitic basalts, reflecting differences in modal plagioclase and clinopyroxene (now amphibole). No fresh olivine has been observed in komatiitic cumulates in the TGB, however, the most primitive low-porosity dunite sample has a whole-rock Mg# of 90 which should approximate the average Fo contents of cumulus olivine in the sample (e.g., Arndt et al. 2008).

Base-metal contents of mafic-ultramafic rocks are low with Cu and Zn both <200 ppm. Highest Ni values of 2500 ppm are associated with olivine cumulates. Pd and Pt are generally below 10 ppb

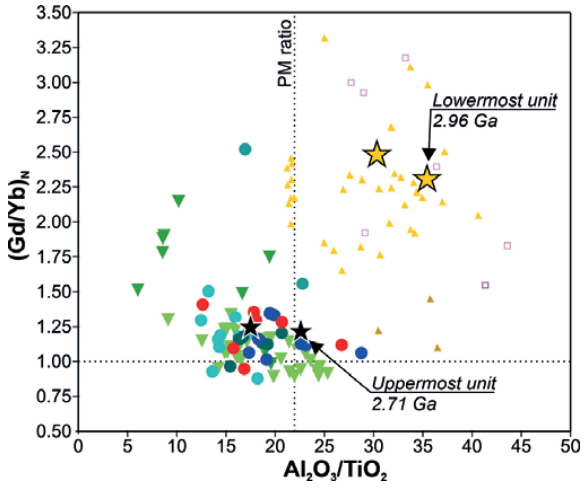


Figure 8. Whole-rock samples from the Takanen greenstone belt on a $(Gd/Yb)_N$ vs. $Al_2O_3/TiO_2$ diagram. Komatiitic samples plot as Al-undepleted komatiites (Arndt et al. 2008). Normalization values from McDonough & Sun (1995). Colors and symbols as in Fig. 6. Units with zircon U-Pb samples marked with stars.

(highest 25 ppb). Au is generally below 10 ppb but about twenty samples show slightly anomalous values of 25–120 ppb ( see S1).

## 5.3 Isotope analyses

### 5.3.1 U-Pb results

Results of single-grain zircon U-Pb isotope analyses of two dated samples (Table 1) can be found in Appendix S1 and are summarized in Fig. 10.

Sample A2611 is from the upper parts of the stratigraphically lowermost felsic volcanic unit of the TGB (Figs. 3e, 4). Its zircon population is characterized by zoned and partly metamict zircon grains, some of which display core-rim structures (Figs. 9c, d). A total of 61 spot analyses from 43 zircon grains were made. Some results plot above

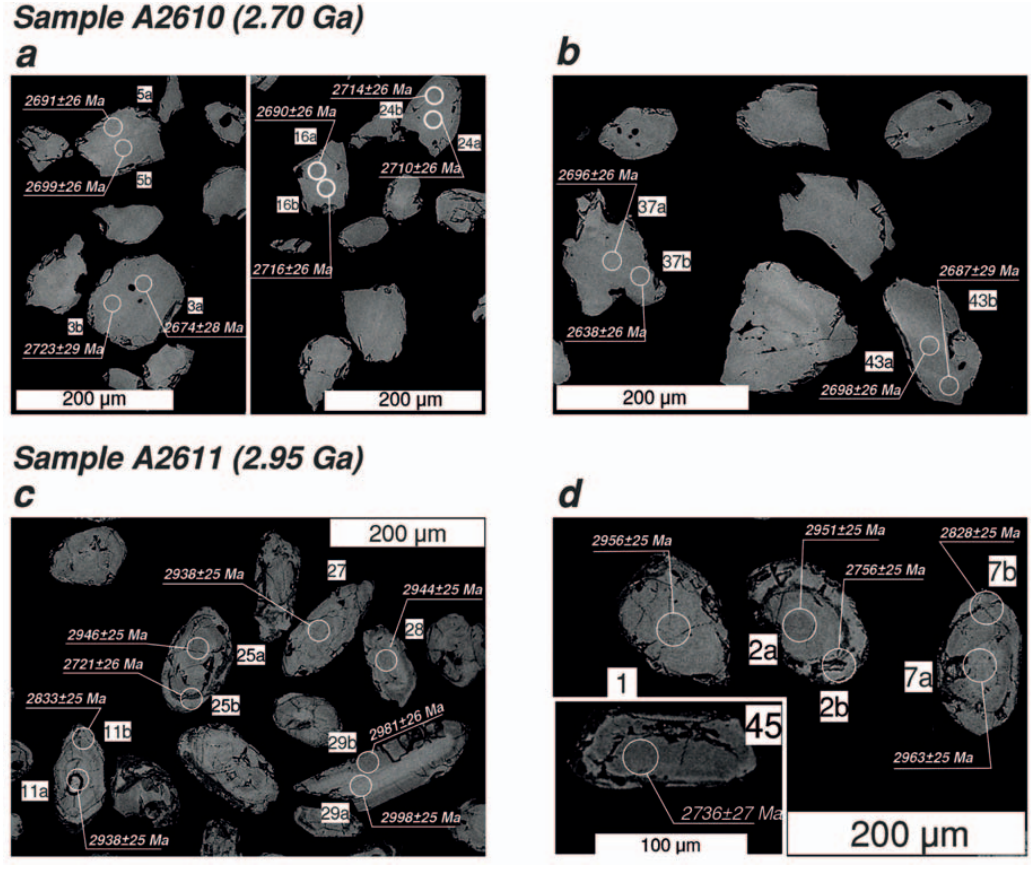


Figure 9. Backscattered electron images of selected zircon grains from (a–b) sample A2610 and (c–d) sample A2611; see Table 1. Laser ablation spot locations for U-Pb and Lu-Hf isotope analyses indicated with white circles and labeled with obtained $^{207}Pb/^{206}Pb$ ages and 1σ-errors.

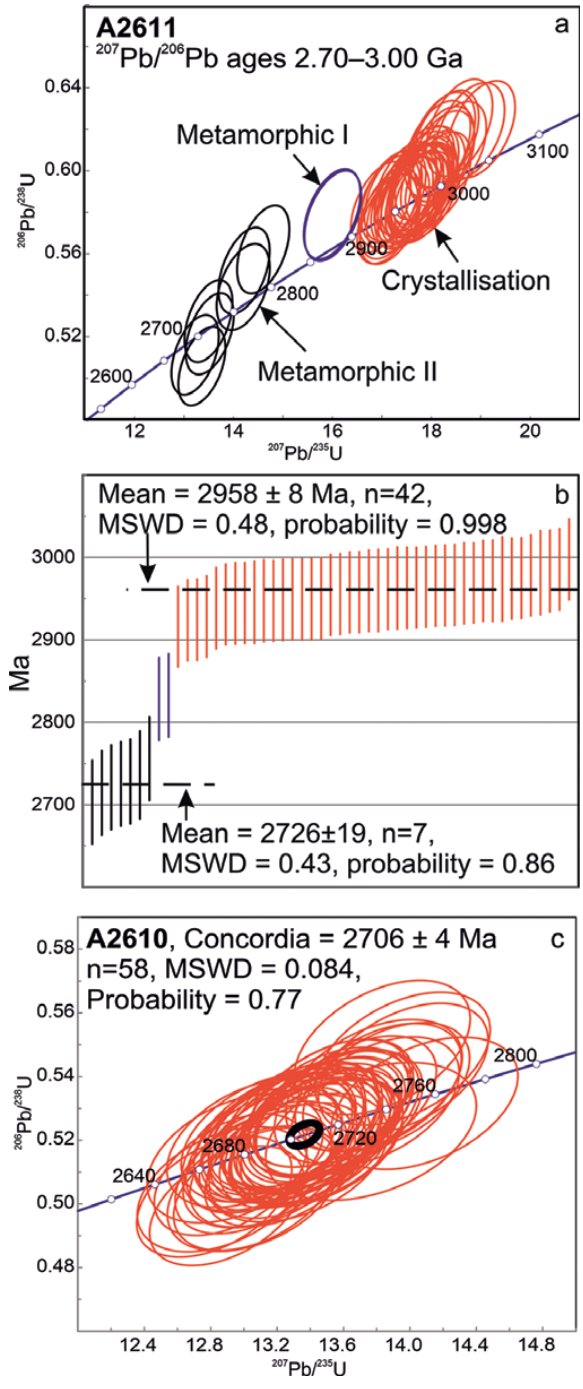


Figure 10. a) Concordia diagram for age determination sample A2611, indicating the three identified age populations. b) $^{207}$Pb/$^{206}$Pb ages for sample A2611 with the averages calculated for the oldest and youngest age group. c) Concordia diagram for sample A2610. See text for further discussion. Error symbols at 2σ level.

the concordia (Fig. 10a). This is attributed to matrix effects in the partially metamict zircon, resulting in fractionation of U during sample ablation and analysis. Although lead isotopes are unaffected by these effects, and thus the $^{207}$Pb/$^{206}$Pb ages for the zircons could be considered trustworthy (see A1772 in Huhma et al. 2012a), we excluded all analyses (n=9) with concordancy >105%. Additionally, one analysis with high common lead was discarded. The remaining 51 analyses display $^{207}$Pb/$^{206}$Pb ages ranging from 2.70 to 3.00 Ga, and form three distinct groups: 3.00–2.92 Ga, ~2.83 Ga, and 2.76–2.70 Ga (Fig. 10a). Weighted average for the oldest group is 2958 ± 8 Ma and for the youngest group 2726 ± 19 Ma (Fig. 10b). Ages from grain rims fall in all three groups, but are more abundant in the two younger groups, in which 5 out of 7 and 2 out of 2 analyses are from rims. Average Th/U for the oldest group is 0.59 and for the youngest group 0.07 (excluding one outlier at 1.81), values which are characteristic for magmatic and metamorphic zircons, respectively (Rubatto & Hermann 2017). Based on the clearly differing age groups, zircon morphology, and U/Th ratios, we interpret the oldest age (2.96 Ga) as the igneous crystallization age of the felsic volcanic unit, and the two younger ages as resetting of the U-Pb system and/or overgrowths caused by younger thermal events.

Sample A2610 is from the stratigraphically uppermost felsic-intermediate volcanic unit of the TGB (Fig. 3b). Zircon grains do not display clear oscillatory zoning (Figs. 9a, b). Total of 62 spots from 50 grains were analyzed. One grain was excluded as obvious contamination (dated 0.67 Ga), and two analyses were excluded based on high common lead content. The remaining 58 analyses show Th/U between 0.17–0.75 (average 0.38) and define a concordia age of 2706 ± 4 Ma (Fig. 10c). We interpret this (2.71 Ga) as the igneous crystallization age of the rock.

### 5.3.2 Lu-Hf results

A total of 21 zircon grains from the two dated samples were measured for their Lu-Hf isotope

composition. Results can be found in Appendix S1. Figure 11a–b displays the initial Hf isotope compositions of the samples expressed as weighted mean $\varepsilon_{Hf}$ values calculated assuming ± 1.6 ε-units as the external 2σ reproducibility based on the GJ-1 reference zircon results. The weighted average of the initial $\varepsilon_{Hf}$ value for sample A2611 is -4.4 ± 1.0 (2σ) at 2.95 Ga, and for sample A2610 it is 1.0 ± 0.8 (2σ) at 2.70 Ga. These are robust values and probably deliver reasonable initial isotope compositions for the two intermediate/silicic magmatic events. All analyzed zircon grains from the upper sample A2610 are from the core parts of the grain, have escaped post-emplacement resetting by subsequent thermal events, and define a near-chondritic initial Hf isotope composition for this magmatic event. In contrast, U-Pb systematics of 4 of the 13 spots analyzed from zircon grains in sample A2611 have been reset close to 2.75 Ga (Fig. 10a–b), but their Lu-Hf isotope system has remained closed as they plot along the $^{176}Hf/^{177}Hf$ evolution paths of crystals that have not been reset (Fig. 11c). This highlights the importance of the Lu-Hf isotope system as a proxy of source components in systems in which the U-Pb system has not remained closed (cf. Andersen 2012; Pokki et al. 2013).

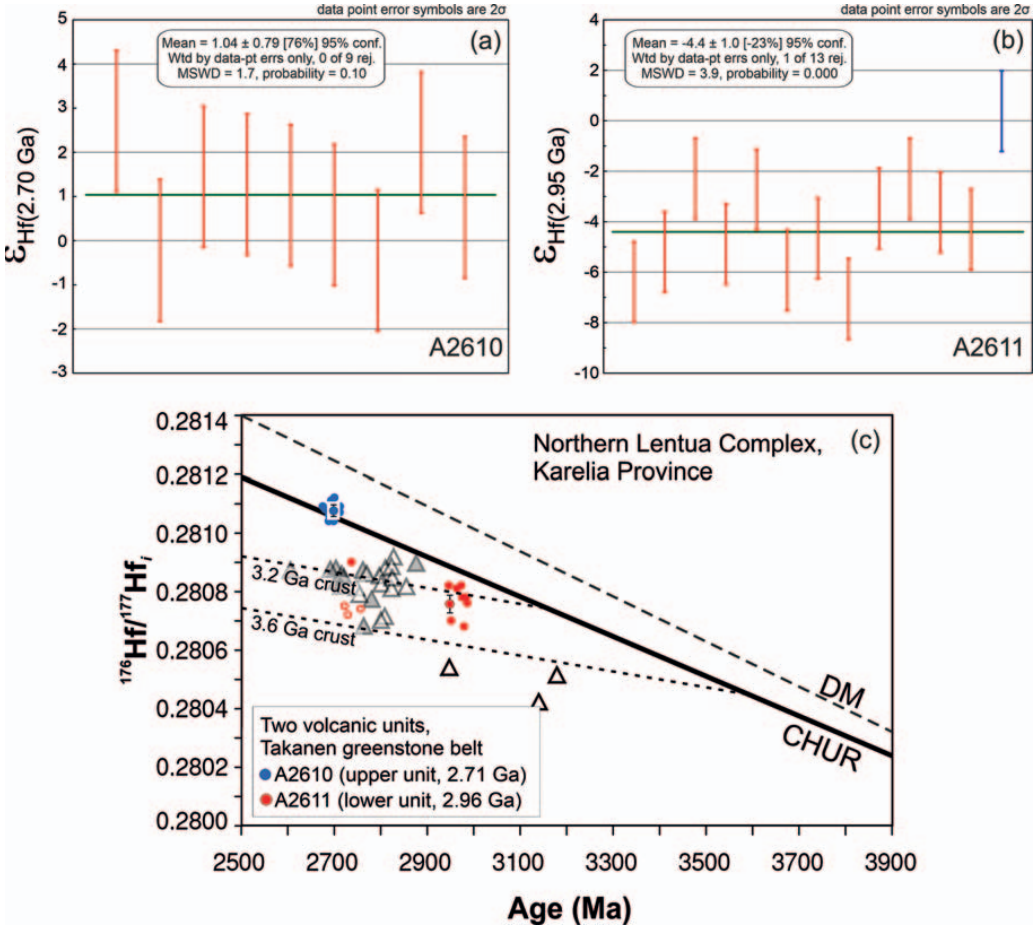


Figure 11. Weighted averages of initial $\varepsilon_{Hf}$ values of individual spots for A2610 and A2611 in sequential order (a–b). c) Weighted average of the initial $^{176}Hf/^{177}Hf$ ratios for the two samples with 2σ error-bars; individual zircon spot-analyses shown in the background (open circle = rim; filled = core). CHUR is the Chondritic Uniform Reservoir (Bouvier et al. 2008), DM is the global depleted mantle (Griffin et al. 2000). White and grey triangles are data form leucogranite and pyroxene tonalite samples from the northern Lentua Complex; these, and evolution paths for two crustal domains extracted from CHUR at 3.6 and 3.2 Ga, are from Lauri et al. (2011).

# 6. Discussion

## 6.1 U-Pb age and Hf-isotope systematics and comparisons

The 2.96 Ga crystallization age obtained for the stratigraphically lowermost felsic volcanic unit of the Takanen greenstone belt (TGB; sample A2611) is similar to the oldest ~2.94 Ga ages obtained from the Suomussalmi greenstone belt (Lehtonen et al. 2017) and enforces the interpretation of the TGB as its direct continuation. Oldest TTG gneisses of the Lentua complex display similar ages (Fig. 2a). The existence of ≥2.95 Ga granitoid crust in northern parts of the Lentua complex is well established based on igneous crystallization ages, inherited zircons (<3.2 Ga), and $T_{DM}$ ages of >3.0 Ga (Mikkola et al. 2011, Hölttä et al. 2021). Our Lu-Hf data from A2611 provides further evidence for existence of, and contribution from, pre-existing (~3.2 Ga) Mesoarchean crust (Fig. 11c). The youngest age group of sample A2611 (2.73 Ga) is likely linked to a metamorphic episode with growth of new low Th/U zircon, which in-turn may be associated with the 2.71 Ga silicic magmatism found at the stratigraphic top of the TGB (sample A2610 below) as both events yield U-Pb ages overlapping within error (Fig. 10a). It would appear that the Lu-Hf isotope system is robust and remained closed in A2611, even when the U-Pb isotope system of some zircon rims has been reset at ~2.7 Ga (Fig. 11c).

The 2.71 Ga crystallization age obtained from the stratigraphically uppermost felsic-intermediate volcanic unit of the TGB (sample A2610) has not previously been reported from volcanic rocks in the Western Karelia Subprovince (WKS); however, plutonic rocks of the same age are common both in Lentua and adjacent complexes (Hölttä & Mänttäri 2002, Lauri et al. 2011, Mikkola et al. 2011; Hölttä et al. 2021). Metasedimentary units with maximum depositional ages of ~2.7 Ga are found south of the TGB (Kontinen et al. 2007; Huhma et al. 2012a) and could be sourced from 2.71 Ga volcanics such as in the TGB. The near-chondritic Lu-Hf data (eHf +1.0) suggests a clearly more juvenile source for the 2.71 Ga succession than for the 2.96 Ga one (Fig. 11c). Also, the relatively high contents of Ni and Cr (Figs. 6h, i) indicate mantle-affinity for the 2.71 Ga unit. Compared to the previously described 2.72–2.70 Ga granitoid magmatism interpreted as being sourced from mantle (sanukitoids, QQs; Heilimo et al. 2010, Mikkola et al. 2011), the 2.71 Ga unit shows very weakly fractionated REE with $(La/Yb)_N$ of 2 compared to 6–15 of the granitoids. Thus, the 2.71 Ga unit in the TGB thus provides a compositionally juvenile addition to this last major crust forming event in the WKS.

Volcanic rocks of the 2.70–2.75 Ga age group are more abundant in the Central Karelia Province (CKS). The Khedozero-Bolshozero greenstone belt (Fig. 1) bears similarities to the younger 2.71 Ga part of the TGB: (1) U-Pb age of 2.71–2.70 Ga; (2) similar lithological association comprising basalt, andesite, dacite, rhyolite (so-called BADR-suite) but missing komatiitic rocks; (3) near-chondritic initial $\varepsilon_{Nd}$ of 0.3–2.6 but with strongly fractionated LREE (Myskova et al. 2020). Volcanic rocks in the Khedozero-Bolshozero belt are LREE-enriched and have been suggested as extrusive equivalents of sanukitoids (Myskova et al. 2020).

## 6.2 Depositional setting

The TGB is composed primarily of rocks of the BADR-suite (basalt-andesite-dacite-rhyolite) with komatiites and komatiitic basalts. The BADR-with-komatiites–association is common in Archean greenstone belts in northern Fennoscandia and is commonly attributed to a plume-tectonic geodynamic model, whereby the BADR-suite is related to a subduction or collisional setting in a continental margin or island-arc and the komatiitic rocks to mantle-plume input (Hölttä et al. 2014; Vrevskii 2019; Myskova et al. 2020; Slabunov et al. 2021).

Rocks of the Takanen greenstone belt have been deformed and overprinted by at least one metamorphic event and only broad interpretations regarding their depositional setting are suggested. Plume-input is inferred from presence of komatiitic

flows in both older and younger parts of the TGB (Fig. 3b). No platform, pelagic, or fluvial-alluvial metasediments (pelites, blackschist, carbonate-rocks, quartzites, conglomerates) are identified. The calc-alkaline succession in the TGB does not contain coarse volcanic breccias or lavas (i.e., proximal volcanic facies), and thus likely represents fine-grained distal ash fall deposits and resedimented volcaniclastic deposits likely mixed with epiclastic material, that is, poorly differentiated immature sediments, e.g., metatuffites or metagraywackes (cf. Slabunov et al. 2021). Komatiites and tholeiitic basalts with (uncertain) pillow structures indicate sub-aqueous deposition. Barren massive Fe-sulfide layers have not been described from other Finnish greenstone belts but are known elsewhere (e.g., Kohler & Anhaeusser 2002; Polito et al. 2007). The Fe-sulfide layers in the TGB may represent magmatic-hydrothermal exhalative chemical sediments (i.e., sulfide-facies banded iron formation; Pirajno & Yu 2021), and thus they may indicate the position of the paleo-seafloor during inter-eruptive volcanic hiatuses.

In the older part of the TGB, a crustal contamination signature is found in some tholeiitic-komatiitic basalt samples (Fig. 7c) suggesting a rift-setting (similar to Suomussalmi; Papunen et al. 2009). This interpretation is hampered by the lack of low detection limit ICP-MS data for most trace elements other than the REE (S1). Furthermore, inferring crustal contamination from metamorphosed extrusive rocks that may have been contaminated during volcanic or sedimentary processes (tuffites) is problematic. The contaminated and non-contaminated metabasalts in our sample set show similar lithologies and textures (Fig. 5e) suggesting contamination during igneous processes. Judging from the relatively small amount and scattered stratigraphic position of LREE-enriched basalt samples, crustal contamination may have been a relatively small-scale or localized process.

Trace-element characteristics of the younger part of the TGB are similar with so called "hot rhyolites" (group F*IV* in Hart et al. 2004), with the

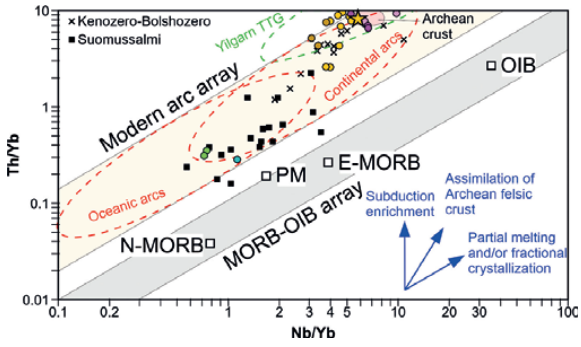


Figure 12. Whole-rock Nb/Yb vs. Th/Yb diagram illustrating subduction vs. mantle-plume signatures in the Takanen belt (colors as in Fig. 6; age dating sample A2611 marked with yellow star); comparisons from Suomussalmi (Kiannaniemi locality) and Khedozero-Bolshozero greenstone belts (Papunen et al. 2009; Myskova et al. 2020). In this study, Nb analyses are only available from drill hole R339 (Fig. 3e). Arrays and mantle sources (N-MORB, PM, E-MORB, OIB) after Smithies et al. (2018).

major difference that the samples from the TGB are andesitic-dacitic and not rhyolitic (60 wt.% vs. 70 wt.% of SiO2). Petrogenesis of "hot rhyolites" has been interpreted to occur in the shallow crust (<15 km deep) with heat for partial melting supplied by, e.g., mafic-ultramafic intrusions in an extensional setting (Hart et al. 2004). Such "hot rhyolites" are considered highly prospective for VMS deposits.

Overall, for the older part of the TGB, the thinly intercalated calc-alkaline and (partly contaminated) tholeiitic-komatiitic rocks suggest a sub-aqueous setting distal to an arc-type volcanic front, or a rift-type setting with bi-modal magmatism, both with plume-input. For the younger part of the TGB, the juvenile isotope and geochemical characteristics of the unit suggest an arc-type (back-arc rift) or oceanic plateau setting, with the former favored as the lithological association is dominated by calc-alkaline felsic-intermediate volcaniclastic rocks (BADR-suite).

The calc-alkaline and tholeiitic-komatiitic rocks of TGB are thinly intercalated, a configuration unlikely to be caused by post-depositional tectonic juxtaposition. To explain the roughly cotemporaneous arc-type and plume-type magmatism in the TGB, two other options are

presented: (1) the previously mentioned plume-tectonics model with coeval mantle plume and (possibly episodic) subduction related magmatism (Grove & Parman 2004; Moyen & Van Hunen 2012; Rehm et al. 2021); or (2) mantle-plume AFC processes with tholeiitic basaltic magma being contaminated with TTG crust (Barnes & Kranendonk 2014; Vrevskii 2019). Discriminating between subduction and plume-AFC models is dependent on the timing of crustal contamination relative to melt production (Smithies et al. 2018). In subduction models, metasomatism of the mantle wedge by mobile elements sourced from a dehydrating plate occurs prior to melting, whereas in plume-AFC–models contamination occurs during assimilation of crustal material after primary melts have already been produced. Nb/Yb vs. Th/Yb plots may discriminate between these effects (Smithies et al. 2018). This is illustrated for Takanen in Fig. 12 where the analyzed samples plot within the continental arc-array; however, only a few low-detection limit Nb-Th analyses are available from the TGB (all from R339; see S1), and thus the results are provisional only.

## 6.3 Stratigraphic correlations and implications

The contact between the lowermost 2.96 Ga felsic volcanic unit of the TGB and the underlying TTGs appears texturally gradational in the only drill core transecting it (Fig. 4). As no tectonic contact is observed, and the presence of >2.95 Ga TTG crust in the northern Lentua complex has been routinely inferred, we tentatively suggest that the basal unit of the TGB may have been deposited (non-conformably) on exhumed plutonic TTG basement. However, the underlying TTG will need to be dated to further test this hypothesis.

An age difference of approximately 250 My and differing trace-element characteristics between the lower (<2.96 Ga) and upper (2.71 Ga) parts of the TGB stratigraphy (Figs. 7e, 8) indicate that the belt is comprised rocks formed in at least two individual events, likely in differing tectonic settings, as has been previously inferred for the nearby Suomussalmi belt composed of a ~2.94 Ga and a 2.84–2.82 Ga component (Lehtonen et al. 2017). The upper and lower parts of the TGB are either tectonically accreted or they are separated by a depositional unconformity, obscured by younger deformation and metamorphism. In the latter case, the older and younger parts of the TGB would be expected to be separated by an orogenic cycle comprising burial, metamorphism, and exhumation, followed by deposition of the 2.71 Ga succession on the <2.96 Ga greenstone association. The two 2.83 Ga zircon rims in sample A2611 (S1) may record this older metamorphic event, if they are not caused by partial resetting of U–Pb systematics of older grains during the 2.7 Ga event. Note that the stratigraphic thickness of the younger 2.71 Ga unit of the TGB remains poorly constrained as the current interpretation is based solely on the distinct REE-pattern of this unit (Fig. 7e; see section 5.2).

Stratigraphic correlations between the Takanen and the Suomussalmi greenstone belts are suggested based on similar lithological associations and U-Pb ages. The 2.96 Ga basal felsic volcanic unit of the TGB can be correlated to the lowermost stratigraphic unit in the Suomussalmi greenstone belt, the Luoma Formation. Luoma is 50–1000 m thick and consists of felsic and intermediate volcanic rocks, tuffs, tuffites, mafic lavas, sedimentary interlayers, and minor komatiite flows and serpentinites with an age of 2.94 Ga (Luukkonen et al. 2002; Papunen et al. 2009; Huhma et al. 2012a; Lehtonen et al. 2017). The up to 100-m-thick differentiated and non-differentiated komatiitic cumulates of the TGB are geochemically and lithologically similar to the Kellojärvi ultramafic cumulate complex and they may thus correlate to the 2793±3 Ma Siivikko Formation in the Kuhmo belt (Fig. 1) (Papunen et al. 2009; Lehtonen et al. 2016). The Cr-basalts found at the top of Siivikko (Halkoaho et al. 2000) are, however, not found in Takanen.

For the 2.71 Ga upper part of the TGB, we interpret it as part of a juvenile plume-influenced arc-system. We suggest a correlation to the 2.71–

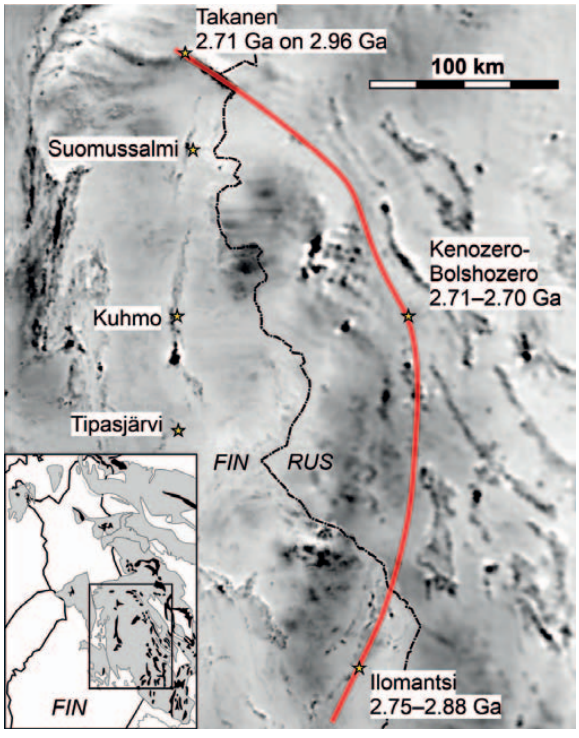


Figure 13. Suggested correlation of the younger (2.71 Ga) part of the Takanen greenstone belt with the 2.75–2.70 Ga Kenozero-Bolshozero and Ilomantsi greenstone belts illustrated on an aeromagnetic map (Korhonen et al. 2002; see also Kulikov et al. 2017). Box in inset shows area in geophysical map (cf. Fig. 1).

2.70 Ga Kenoshero-Bolshozero belt (Myskova et al. 2020) and further to the 2.88–2.75 Ga Ilomantsi belt (Sorjonen-Ward 1993; Huhma et al. 2012a). On the aeromagnetic map in Fig. 13, the Takanen–Kenoshero-Bolshozero–Ilomantsi belts would form a curvilinear 2.75–2.70 Ga orogenic margin that roughly follows the boundary between the Western and Central Karelia Subprovinces as proposed by Hölttä et al. (2012a) (cf. Fig. 1). We suggest that the TGB marks the northwestern part of this subprovince boundary.

A general correlation between the Archean Karelia and Superior cratons has been suggested based on similar ages and characters of Archean TTGs and greenstone sequences (Stone 2005; Strong et al. 2022, 2023; see also Ernst & Bleeker 2010). A model indicating rifting of the Archean Superior proto-craton at 3.0–2.9 Ga followed by collision and orogeny at 2.7 Ga has been suggested (Strong et al. 2023). A similar model for the WKS can be tentatively suggested based on our results, with the lowest parts of both the Takanen and Suomussalmi belts possibly representing rifting of the Karelia craton at ~2.95 Ga, followed by collisional arc-magmatism at 2.75–2.70 Ga in a craton-wide orogeny, represented, in part, by the margin in Fig. 13. The older part of the Takanen greenstone belt was deformed and the U-Pb system partly overprinted by this ~2.7 Ga orogenic event. The younger part would then have been deposited unconformably on top of the older part of the belt.

## 6.4 Komatiite volcanology and Ni-potential

Komatiite facies in the Takanen greenstone belt varies from 1) thin flows (1–10 m) intercalated with other rock types to 2) at least 80 m-thick differentiated pooled flows or sills showing differentiation from peridotite to gabbro, to 3) undifferentiated dunitic cumulates interpreted as bases of channelized flows (Fig. 5l) (Gole & Barnes 2020). Dunitic channel-facies cumulates with both high MgO and low Cr have been previously interpreted as highly prospective (Barnes 1998; Konnunaho 2016) but such rock compositions have not been found in this study. The MgO vs. Cr diagram in Fig. 14a indicates that all the Takanen komatiitic cumulates contain both olivine and chromite. The presence of chromite in a komatiitic cumulate can be used as a general proxy for the temperature of the original komatiitic magma. Chromite saturation in komatiitic magma is typically reached with decreasing temperature at approximately $Fo_{92–93}$ (Barnes 1998). Therefore, the absence of chromite-free olivine cumulates (Fig. 14a) suggests that the komatiitic cumulates in Takanen were formed from a relatively evolved and cool (low-MgO and low-Fo) komatiitic magma. Decrease in the magma temperature decreases the capacity of komatiitic magma to assimilate sulfidic footwall rocks (Lesher & Keays 2002).

Some komatiitic samples from relatively thin

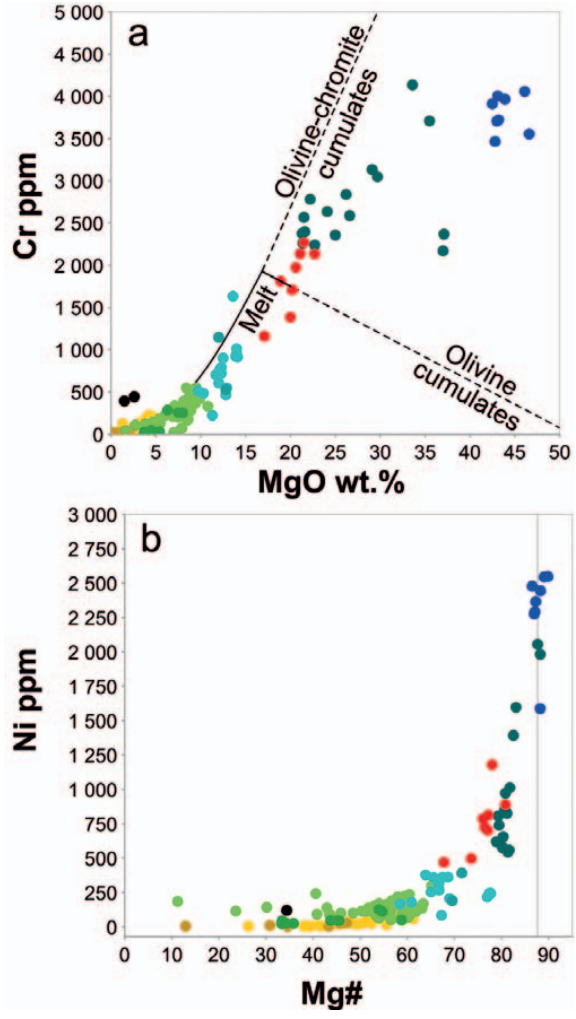


Figure 14. Whole-rock compositions of komatiites in Takanen belt a) on a MgO vs Cr plot illustrating chromite-systematics of cumulates (colors as in Fig. 6). High MgO samples (>40 wt.%) plot as olivine-chromite cumulates and lower MgO samples (<35 wt.% MgO) as olivine-pyroxene-chromite cumulates. Samples with red markers likely approximate the komatiitic parental melt composition in Takanen with c. 20 wt.% MgO. A fractional crystallization curve of a komatiitic parental liquid with ~20 wt MgO shown in black, with trajectories in dashed lines illustrating fractionation of olivine-only and olivine-chromite cumulates (e.g., Barnes 1998). b) Mg# vs Ni plot illustrating Ni-depletion in komatiitic cumulates (Ni values range between 1500–2500 ppm at Mg# of about 90).

flow units have whole-rock compositions with ~20 wt.% MgO with melt-like incompatible element content (Fig. 6) and flat PM-normative REE-patterns (Fig. 7a). We interpret these samples to approximate the parental komatiite melt composition in Takanen. Similar relatively low-MgO komatiitic parental melt has been suggested for the Kellojärvi cumulate complex of the Kuhmo belt (Papunen et al. 2009).

As noted by Guo et al. (2020), Archean komatiites in Karelia appear to be relatively MgO-poor (low-temperature) in comparison to those in Canada and Western Australia, and this might explain their lower economic endowment. Nevertheless, in Takanen the komatiitic cumulates appear stratigraphically above stratiform sulfide layers (Fig. 3). This setting has potential for assimilation of sulfidic footwall and formation of Ni-sulfide deposits (Lesher & Keays 2002), as exemplified by the Vaara deposit in the neighboring Suomussalmi greenstone belt (Konnunaho et al. 2013). Some evidence of such processes is found in the western parts of the TGB, where a thick differentiated komatiitic cumulate unit shows a 1 m-thick hybridized footwall contact (drill hole KUV-1 in Fig. 3c; Vesanto 2003), however, both units are unmineralized. One olivine adcumulate sample in a neighboring drill hole was found to contain minor pentlandite and nickeline (R324 16.65 m in Fig. 3c; 43 wt.% MgO, 2300 ppm Ni, 1700 ppm S) and some Ni depletion is evident in the Takanen komatiites (Fig. 14b). This should be scrutinized in further contributions to Takanen geology.

# 7. Conclusions

- The Archean Takanen greenstone belt consists of an at least 800-m-thick succession dominated by basaltic-komatiitic flows and mafic-felsic volcaniclastic rocks, the latter likely including both pyroclastic and resedimented volcanogenic material. Massive Fe-sulfide layers <1-m-thick are associated with volcaniclastic units. The belt is intruded by several sets of granitoid dykes.
- A felsic volcanic unit from the stratigraphic base of the belt provides a crystallization age

of 2.96 Ga. Based on the age and lithologic context this unit is correlated with the ~2.94 Ga Luoma-group in the Suomussalmi greenstone belt.
- A felsic-intermediate volcanic unit from the uppermost stratigraphic part of the belt provides a crystallization age of 2.71 Ga. Volcanic rocks of this age group have not previously been reported from the Western Karelia Subprovince. We tentatively suggest a correlation to the 2.71–2.70 Ga Khedozero-Bolshozero greenstone belt in the Central Karelia Subprovince.
- Hf-isotope compositions of analyzed zircons suggest that the 2.96 Ga sample contains material from an older source, possibly ~3.2 Ga TTG crust. In contrast, the 2.7 Ga sample has a near-chrondritic juvenile isotopic composition.
- Different ages, trace-element, and isotopic compositions between the lower and upper parts of the Takanen greenstone belt stratigraphy suggest a secular change in magma source and a different tectonic setting for the lower and upper parts of the Takanen greenstone belt stratigraphy. Despite a ~250 Ma age difference, no contact or unconformity between the lower and upper parts has been observed.
- The 2.71 Ga sample indicates an episode of juvenile crust formation at ~2.7 Ga in the northern Lentua complex, similar to what has been previously described from the southern part of the Lentua complex as well as from the neighboring Pudasjärvi and Ilomantsi complexes.
- Channelized komatiitic cumulates are found overlying volcaniclastic rocks which host stratiform Fe-sulfide horizons, a configuration with high potential for komatiite-hosted Ni-deposits. Ni-potential may be downgraded by the relatively low inferred temperature (and thus decreased assimilation potential) of the komatiitic parental magma (~20 wt.% MgO and $Fo_{90}$).

# Acknowledgements

We thank the staff of the Isotope laboratory of the Geological Survey of Finland for sample preparation, and Matti Kurhila for tabulating the isotope geochemical results. The manuscript greatly benefited from reviews by P. Hölttä and P. C. Thurston, and from the helpful comments provided by the journal editors J. Kohonen and A. Slabunov.

# Supplementary Data

Electronic Appendices are available via Bulletin of the Geological Society Finland web page.

Electronic Appendix A: S1 Results of whole-rock geochemical analyses, and singe-grain zircon LA-ICP-MS U-Pb and Lu-Hf isotope analysis results and method descriptions.

# References

Alapieti, T., 1982. The Koillismaa layered igneous complex, Finland - its structure, mineralogy and geochemistry, with emphasis on the distribution of chromium. Geological Survey of Finland, Bulletin 319, 116 p.

Andersen, T., 2012. Age, Hf isotope and trace element signatures of detrital zircons in the Mesoproterozoic Eriksfjord sandstone, southern Greenland: are detrital zircons reliable guides to sedimentary provenance and timing of deposition? Geological Magazine 150, 426–440. https://.doi.org/10.1017/S0016756812000623

Arndt, N., Lesher, C. M. & Barnes, S. J., 2008: Komatiite. Cambridge University Press, Cambridge. 467 p. https://doi.org/10.1017/CBO9780511535550

Barnes, S. J., 1998. Chromite in komatiites, 1. Magmatic controls on crystallization and composition. Journal of Petrology 39, 1689–1720. https://doi.org/10.1093/petroj/39.10.1689

Barnes, S. J. & Van Kranendonk, M., 2014. Archean andesites in the east Yilgarn craton Australia: products of plume-related interaction? Lithosphere 6, 80–92. https://doi.org/10.1130/L356.1

Bedrock of Finland – DigiKP. Digital map database [electronic resource, referred November 2021]. Geological Survey of Finland, Espoo, scale-free version, available at https://gtkdata.gtk.fi/Kalliopera/index.html

Belousova, E. A., Griffin, W. L. & O'Reilly, S. Y., 2006. Zircon crystal morphology, trace element signatures and Hf isotope composition as a tool for petrogenetic modeling: examples from Eastern Australian granitoids. Journal of Petrology 47, 329–353. https://doi.org/10.1093/petrology/egi077

Bleeker, W., 2002. Archean tectonics: a review, with illustrations from the Slave craton. In: Fowler, C., M., R. et al. (eds.) The Early Earth: Physical, Chemical and Biological Development. Geological Society of London, Special Publications 199, 151–181. https://doi.org/10.1144/GSL.SP.2002.199.01.09

Bouvier, A., Vervoort, J. D. & Patchett, P. J., 2008. The Lu–Hf and Sm–Nd isotopic composition of CHUR: Constraints from unequilibrated chondrites and implications for the bulk composition of terrestrial planets. Earth and Planetary Science Letters 273, 48–57. https://doi.org/10.1016/j.epsl.2008.06.010

Condie, K. C., 2014. How to Make a Continent: Thirty-five years of TTG Research. In: Dilek, Y. & Furnes, H. (eds.) Evolution of Archean Crust and Early Life, Modern Approaches in Solid Earth Sciences 7. Springer. https://doi.org/10.1007/978-94-007-7615-9_7

Ernst, R. E. & Bleeker, W., 2010. Large igneous provinces (LIPs), giant dyke swarms, and mantle plumes: significance for breakup events within Canada and adjacent regions from 2.5 Ga to the Present. Canadian Journal of Earth Sciences 47, 695–739. https://doi.org/10.1139/E10-025

Gole, M. J. & Barnes, S. J., 2020. The association between Ni-Cu-PGE sulfide and Ni-Co lateritic ores and volcanic facies within the komatiites of the 2.7 Ga East Yilgarn Craton large igneous province, Western Australia. Ore Geology Reviews 116, 1–21. https://doi.org/10.1016/j.oregeorev.2019.103231

Griffin, W. L., Pearson, N.J., Belousova, E., Jackson, S. E., van Achterbergh, E., O'Reilly, S. Y. & Shee, S. R., 2000. The Hf isotope composition of cratonic mantle: LAM-MC-ICPMS analysis of zircon megacrysts in kimberlites. Geochimica et Cosmochimica Acta 64, 133–147. https://doi.org/10.1016/S0016-7037(99)00343-9

Grove, T. L. & Parman, S. W., 2004. Thermal evolution of the Earth as recorded by komatiites. Earth and Planetary Science Letters 219, 173–187. https://doi.org/10.1016/S0012-821X(04)00002-0

Guo, F. F,, Svetov, S., Maier, W. D., Hanski, E., Yang, S. H. & Rybnikova, Z., 2020. Geochemistry of komatiites and basalts in Archean greenstone belts of Russian Karelia with emphasis on platinum-group elements. Mineralium Deposita 55, 971–990. https://doi.org/10.1007/s00126-019-00909-0

Halkoaho, T., Liimatainen, J., Papunen, H. & Välimaa, J., 2000. Exceptionally Cr-rich basalts in the komatiitic volcanic association of the Archaean Kuhmo greenstone belt, eastern Finland. Mineralogy and Petrology 70, 105-120. https://doi.org/10.1007/s007100070016

Hart, T. R., Gibson, H. L. & Lesher, C. M., 2004. Trace element geochemistry and petrogenesis of felsic volcanic rocks associated with volcanogenic massive Cu-Zn-Pb sulfide deposits. Economic Geology 99, 1003–1013. https://doi.org/10.2113/gsecongeo.99.5.1003

Heilimo, E., Halla, J. & Hölttä, P., 2010. Discrimination and origin of the sanukitoid series: Geochemical constraints from the Neoarchean western Karelian Province (Finland). Lithos 115, 27–39. https://doi.org/10.1016/j.lithos.2009.11.001

Heilimo, E., Mikkola, P., Ahven, M., Huhma, H., Lahaye, Y., Virtanen, V. J., 2023. Evidence of crustal growth during the Svecofennian orogeny: New isotopic data from the central parts of the Paleoproterozoic Central Finland Granitoid Complex. Precambrian Research 395. https://doi.org/10.1016/j.precamres.2023.107125

Hölttä, P., Heilimo, E., Huhma, H., Kontinen, A., Mertanen, S., Mikkola, P., Paavola, J., Peltonen, P., Semprich, J., Slabunov, A. & Sorjonen-Ward, P., 2012a. The Archaean of the Karelia Province in Finland. Geological Survey of Finland, Special Paper 54, 21–73

Hölttä, P., Heilimo, E., Huhma. H., Juopperi, H., Kontinen, A., Konnunaho, H., Lauri, L., Mikkola, P., Paavola, J. & Sorjonen-Ward, P., 2012b. Archaean complexes of the Karelia Province in Finland. Geological Survey of Finland, Special Paper 54, 9–20.

Hölttä, P., Heilimo, E., Huhma, H., Kontinen, A., Mertanen, S., Mikkola, P., Paavola, J., Peltonen, P., Semprich, J., Slabunov, A., & Sorjonen-Ward, P., 2014. The Archaean Karelia and Belomorian Provinces, Fennoscandian Shield. In: Dilek, Y. & Furnes, H. (eds.) Evolution of Archean Crust and Early Life. Modern Approaches in Solid Earth Sciences, vol 7. Springer. https://doi.org/10.1007/978-94-007-7615-9_3

Hölttä, P., Mänttäri, I., Huhma, H., Kurhila, M., Ruotoistenmäki, T. & Kontinen, A., 2021. Growth of the Archean sialic crust as revealed by zircon in the TTGs in eastern Finland. Bulletin of the Geological Society of Finland 93, 77–104. https://doi.org/10.17741/bgsf/93.2.001

Huhma, H., Kontinen, A., Mikkola, P., Halkoaho, T., Hokkanen, T., Hölttä, P., Juopperi, H., Konnunaho, J., Luukkonen, E., Mutanen, T., Peltonen, P., Pietikäinen, K. & Pulkkinen, A., 2012b. Nd isotopic evidence for Archaean crustal growth in Finland. Geological Survey of Finland, Special Paper 54, 175–212.

Huhma, H., Mänttäri, I., Peltonen, P., Kontinen, A., Halkoaho, T., Hanski, E., Hokkanen, T., Hölttä, P., Juopperi, H., Konnunaho, J., Layahe, Y., Luukkonen, E., Pietikäinen, K., Pulkkinen, A., Sorjonen-Ward, P., Vaasjoki, M. & Whitehouse, M., 2012a. The age of the Archaean greenstone belts in Finland. Geological Survey of Finland, Special Paper 54, 74–175.

Iljina, M., 2003. Hanke 2106001. Pohjois-Suomen kerrosintruusiot 1996–2002 Loppuraportti. Geological Survey of Finland, Archive report M10.4/2003/4, 20 p.

Iljina, M., Salmirinne, H. & Heikura, P., 2006. Tutkimustyöselostus Kuparivaaran valtauksella (7655/1) Kuusamossa suoritetuista tutkimuksista vuosina 2003-2004. Geological Survey of Finland, Archive report M06/4523/2006/1/10, 10 p.

Järvinen, V., 2022. Petrogenesis and orthomagmatic mineral potential of the mafic-ultramafic 2.44 Ga Näränkävaara intrusion, northern Finland. PhD Thesis, University of Helsinki, Finland, 49 p.

Käpyaho, A., Mänttäri, I. & Huhma, H., 2006. Growth of Archaean crust in the Kuhmo district, eastern Finland: U-Pb and Sm-Nd isotope constraints on plutonic rocks. Precambrian Research 146, 95–119. https://doi.org/10.1016/j.precamres.2006.01.006

Käpyaho, A., Hölttä, P., & Whitehouse, M., 2007. U-Pb zircon geochronology of selected Neoarchaean migmatites in eastern Finland. Bulletin of the Geological Society of Finland 79, 95–115. https://doi.org/10.17741/bgsf/79.1.005

Karampelas, N., 2022. Petrography, lithology, geochemistry and geochronology of the Takanen greenstone belt, eastern Finland. MSc. thesis, University of Helsinki, Finland, 79 p.

Karinen, T., 2010. The Koillismaa intrusion, northeastern Finland – evidence for PGE reef forming processes in the layered series. PhD Thesis, Geological Survey of Finland, Bulletin 404, 176 p.

Kohler, E. A. & Anhaeusser, C. R., 2002. Geology and geodynamic setting of Archaean silicic metavolcaniclastic rocks of the Bien Venue Formation Fig Tree Group, northeast Barberton greenstone belt, South Africa. Precambrian Research 116, 199–235. https://doi.org/10.1016/S0301-9268(02)00021-9

Konnunaho, J., 2016. Komatiite-hosted Ni-Cu-PGE deposits in Finland: Their characterization, PGE content, and petrogenesis. PhD Thesis, University of Oulu, 38 p.

Konnunaho, J. P., Hanski, E. J., Bekker, A., Halkoaho, T. A. A., Hiebert, R. S. & Wing, B. A., 2013. The Archean komatiite-hosted, PGE-bearing Ni–Cu sulphide deposit at Vaara, eastern Finland: evidence for assimilation of external sulfur and post-depositional desulfurization. Mineralium Deposita 48, 967–989. https://doi.org/10.1007/s00126-013-0469-0

Kontinen, A., Käpyaho, A., Huhma, H., Karhu, J., Matukov, D. I., Larionov, A. & Sergeev, S. A., 2007. Nurmes paragneisses in eastern Finland Karelian craton: provenance tectonic setting and implications for Neoarchaean craton correlation. Precambrian Research 152, 119–148. https://doi.org/10.1016/j.precamres.2006.11.001

Korhonen, J. V., Aaro, S., All, T., Nevanlinna, H., Skilbrei, J. R., Säävuori, H., Vaher, R., Zhdanova, L. & Koistinen, T., 2002. Magnetic anomaly map of the Fennoscandian Shield. The Geological Surveys of Finland, Norway and Sweden and Ministry of Natural Resources of the Russian Federation.

Kozhevnikov, V. N., Berezhnaya, N. G., Presnyakov, S. L., Lepekhina, E. N., Antonov, A. V. &. Sergeev, S. A., 2006. Geochronology (SHRIMP-II) of zircon from Archean lithotectonic associations in the greenstone belts of the Karelia craton: implications for stratigraphic and geodynamic reconstructions. Stratigraphy and Geological Correlation 14, 240–259. http://doi.org/10.1134/S0869593806030026

Kulikov, V. S., Svetov, S. A., Slabunov, A. I., Kulikova, V. V., Polin, A. K., Golubev, A. I., Gorkovets, V. Y., Ivashchenko, V. I., Gogolev, M. A., 2017. Geological map of Southeastern Fennoscandia (scale 1:750 000): A new approach to map compilation. Karelian Research Centre of the Russian Academy of Sciences, online publication. https://doi.org/10.17076/geo444

Lauri, L. S., Rämö, O. T., Huhma, H., Mänttäri, I. & Räsänen, J., 2006. Petrogenesis of silicic magmatism related to the 2.44 Ga rifting of Archean crust in Koillismaa, eastern Finland. Lithos 86, 137–166. http://doi.org/10.1016/j.lithos.2005.03.016

Lauri, L. S., Andersen, T., Hölttä, P., Huhma, H. & Graham, S., 2011. Evolution of the Archaean Karelian Province in the Fennoscandian Shield in the light of U–Pb zircon ages and Sm–Nd and Lu–Hf isotope systematics. Journal of the Geological Society 168, 201–218. https://doi.org/10.1144/0016-76492009-159

Lehtonen, E. & Käpyaho, A., 2016. A small Archaean belt—diverse age ensemble: a U–Pb study of the Tipasjärvi greenstone belt, Karelia Province, Central Fennoscandian Shield, Finland. Lithos 246–247, 31–47. https://doi.org/10.1016/j.lithos.2015.11.008

Lehtonen, E., Heilimo, E., Halkoaho, T., Käpyaho, A. & Hölttä, P., 2016. U-Pb geochronology of Archaean volcanic-sedimentary sequences in the Kuhmo greenstone belt, Karelia Province – Multiphase volcanism from Meso- to Neoarchaean and a Neoarchaean depositional basin? Precambrian Research 275, 48–69. https://doi.org/10.1016/j.precamres.2015.12.002

Lehtonen, E., Heilimo, E., Halkoaho, T., Hölttä, P. & Huhma, H. 2017. The temporal variation of Mesoarchean volcanism in the Suomussalmi greenstone belt, Karelia Province, Eastern Finland. International Journal of Earth Sciences 106, 763–781. https://doi.org/10.1007/s00531-016-1327-y

Lesher, C. M. & Keays, R. R., 2002. Komatiite-associated Ni-Cu-PGE deposits: Geology, mineralogy, geochemistry and genesis. In: Cabri, L. J. (ed), The Geology, Geochemistry, Mineralogy and Mineral Beneficiation of Platinum-Group Elements. Canadian Institute of Mining, Special Volume 54, 580–617.

Ludwig. K. R., 2003. User's manual for Isoplot/Ex, Version 3.00. A geochronological toolkit for Microsoft Excel. Berkeley Geochronology Center Special Publication No.4.

Luukkonen, E. J., 1992. Late Archaean and early Proterozoic structural evolution in the Kuhmo-Suomussalmi

terrain eastern Finland. University of Turku, Series A II, Biologica-geographica-geologica 78.

Luukkonen, E., Halkoaho, T., Hartikainen, A., Heino, T., Niskanen, M., Pietikäinen, K. & Tenhola, M., 2002. Archaean areas of eastern Finland in the years 1992–2001 in the communities of Suomussalmi, Hyrynsalmi, Kuhmo, Nurmes, Rautavaara, Valtimo, Lieksa, Ilomantsi, Kiihtelysvaara, Eno, Kontiolahti, Tohmajärvi and Tuupovaara. Geological Survey of Finland, Archive report M19/4513/2002/1, 265 p.

Maier, W. D., Peltonen, P., Halkoaho, T. & Hanski, E., 2013. Geochemistry of komatiites from the Tipasjärvi, Kuhmo, Suomussalmi, Ilomantsi and Tulppio greenstone belts, Finland: Implications for tectonic setting and Ni sulphide prospectivity. Precambrian Research 228, 63–84.

Mänttäri, I. & Hölttä, P., 2002. U-Pb dating of zircons and monazites from Archean granulites in Varpaisjärvi, central Finland: evidence for multiple metamorphism and Neoarchean terrane accretion. Precambrian Research 118, 101–131. https://doi.org/10.1016/S0301-9268(02)00094-3

Martin, H., Auvray, B. Blais, S., Capdevila, R., Hameurt, J., Jahn, B.M., Piquet, D., Quérré, G. & Vidal, Ph., 1984. Origin and geodynamic evolution of the Archean crust of eastern Finland. Bulletin of the Geological Society of Finland 56, 135–160. https://doi.org/10.17741/bgsf/56.1-2.009

McDonough, W. F. & Sun S.-S., 1995. The composition of the Earth. Chemical Geology 120, 223–253. https://doi.org/10.1016/0009-2541(94)00140-4

Mikkola, P., Huhma, H., Heilimo, E. & Whitehouse, M., 2011. Archean crustal evolution of the Suomussalmi district as part of the Kianta Complex, Karelia; constraints from geochemistry and isotopes of granitoids. Lithos 125, 287–307. https://doi.org/10.1016/j.lithos.2011.02.012

Mikkola, P., Lauri, L. S. & Käpyaho, A., 2012. Neoarchean leucogranitoids of the Kianta Complex Karelian Province, Finland: source characteristics and processes responsible for the observed heterogeneity. Precambrian Research 206–207, 72–86. https://doi.org/10.1016/j.precamres.2012.02.010

Molnár, F., Middleton, A., Stein, H., O`Brien, H., Lahaye, Y., Huhma, H., Pakkanen, L. & Johanson, B., 2018. Repeated syn- and post-orogenic gold mineralization events between 1.92 and 1.76 Ga along the Kiistala Shear Zone in the Central Lapland Greenstone Belt, northern Finland. Ore Geology Reviews 101, 936–959. https://doi.org/10.1016/j.oregeorev.2018.08.015

Moyen, J.-F. & van Hunen, J., 2012. Short-term episodicity of Archean plate tectonics. Geology 40, 451–454. https://www.doi.org/10.1130/G322894.1

Myskova, T.A., Milkevich, R.I., Lvov, P.A. & Zhitnikova, I., A., 2020. Neoarchean Volcanites of the Khedozero-Bolshozero Greenstone Structure (Central Karelia): Composition, Age, and Tectonic Setting. Stratigraphy and Geological Correlation 28, 107–134. https://doi.org/10.1134/S0869593820020045

Papunen, H., Halkoaho, T. & Luukkonen, E., 2009. Archaean evolution of the Tipasjärvi-Kuhmo-Suomussalmi Greenstone Complex, Finland. Geological Survey of Finland, Bulletin 403, 68 p.

Pirajno, F., Yu, H. C., 2021. Cycles of hydrothermal activity, precipitation of chemical sediments, with special reference to Algoma-type BIF. Gondwana Research 100, 251–260. https://doi.org/10.1016/j.gr.2021.02.012

Pokki, J., Kohonen, J., Rämö O. T. & Andersen, T., 2013. The Suursaari conglomerate (SE Fennoscandian shield; Russia) – Indication of cratonic conditions and rapid reworking of quartz arenitic cover at the outset of the emplacement of the rapakivi granites at ca. 1.65 Ga. Precambrian Research 233, 132–143. https://doi.org/10.1016/j.precamres.2013.04.008

Polito, P., Kyser, K., Lawie, D., Cook, S. & Oates, C., 2007. Application of sulphur isotopes to discriminate Cu-Zn VHMS mineralization from barren Fe sulphide mineralization in the greenschist to granulite facies Flin Flon–Snow Lake–Hargrave River region, Manitoba, Canada. Geochemistry: Exploration, Environment, Analysis 7, 129–138. https://doi.org/10.1144/1467-7873/07-125

Puchtel, I. S., Hofman, A. W., Mezer, K., Jochum, K. P., Shchipansky, A. A. & Samsonov, A. V., 1998. Oceanic plateau model for continental crustal growth in the Archaean: A case study from the Kostomuksha greenstone belt, NW Baltic Shield. Earth and Planetary Science Letters 155, 57–74. https://doi.org/10.1016/S0012-821X(97)00202-1

Rasilainen, K., Lahtinen, R. & Bornhorst, T. J., 2007. The rock geochemical database of Finland manual. Geological Survey of Finland, Report of Investigation 164, 38 p.

Rasilainen, K., Eilu, P., Äikäs, O., Halkoaho, T., Heino, T., Iljina, M., Juopperi, H., Kontinen, A., Kärkkäinen, N., Makkonen, H., Manninen, T., Pietikäinen, K., Räsänen, J., Tiainen, M., Tontti, M. & Törmänen, T. 2012. Quantitative mineral resource assessment of nickel, copper and cobalt in undiscovered Ni-Cu deposits in Finland. Geological Survey of Finland, Report of Investigation 194, 514 p.

Rehm, A. G., Jorgensen, T. R. C., Thurston, P. C., Gibson, H. L. & Lafrance, B., 2021. Synsedimentary rifting and basaltic-komatiitic volcanism in the Pontiac subprovince, Superior craton (Canada): Implications for Neoarchean geodynamics. Precambrian Research 362. https://www.doi.org/10.1016/j.precamres.2021.106204

Rubatto, D. & Hermann, J., 2007. Experimental zircon/melt and zircon/garnet trace element partitioning and implications for the geochronology of crustal rocks. Chemical Geology 241, 38-61. https://doi.org/10.1016/j.chemgeo.2007.01.027

Slabunov, A. I., Lobach-Zhuchenko, S. B., Bibikova, E. V., Sorjonen-Ward, P., Balangansky, V. V., Volodichev, O. I., Shchipansky, A. A., Svetov, S. A., Chekulaev, V. P., Arestova, N. A. & Stepanov, V. S., 2006. The Archaean nucleus of the Baltic/Fennoscandian Shield. In: Gee DG

& Stephenson RA (eds.) European lithosphere dynamics. Geological Society of London Memoir 32, 627–644. https://doi.org/10.1144/gsl.mem.2006.035.01.37

Slabunov, A.I., Nesterova, N.S., Egorov, A.V., Kuleshevich, L. V. Kevlich, V. I., 2021. Age of the Archean Strata with Banded Iron Formation in the Kostomuksha Greenstone Belt, Karelian Craton, Fennoscandian Shield: Constraints on the Geochemistry and Geochronology of Zircons. Geochemistry International 59, 341–356. https://doi.org/10.1134/S0016702921040066

Smithies, R. H., Ivanic, T. R., Lowrey, J. R., Morris, P. A., Barnes, S. J., Wyche, S. & Lu, Y.-J., 2018. Two distinct origins for Archean greenstone belts. Earth and Planetary Science Letters 48, 106–116. https://doi.org/10.1016/j.epsl.2018.01.034

Sorjonen-Ward, P., 1993. An overview of structural evolution and lithic units within and intruding the late Archean Hattu schist belt Ilomantsi eastern Finland. Geological Survey of Finland, Special Paper 17, 9–102.

Stone, D., 2005. Geology of the northern Superior area, Ontario. Ontario Geological Survey, Open File Report 6140, 94 p.

Strong, J. W. D., Mulder, J., Cawood, P. A., Cruden, A. R. & Nebel, O., 2023. Isotope evidence for Archean accordion-tectonics in the Superior Province. Precambrian Research 393. https://doi.org/10.1016/j.precamres.2023.107096

Strong, J. W. D. Cawood, P. A., Cruden, A. R., Nebel, O. Mulder, J. & Dickin, A. P., 2022. Forging isotopically juvenile metamorphic zircon from and within Archean TTG gneiss: Whole-rock Sr-Nd-Pb and zircon U-Pb-Hf-REE constraints. Chemical Geology 590. https://doi.org/10.1016/j.chemgeo.2022.120710

Thurston, P. C., 2002. Autochthonous development of Superior Province greenstone belts? Precambrian Research 115, 11–36. https://doi.org/10.1016/S0301-9268(02)00004-9

Thurston, P. C., 2015. Igneous Rock Associations 19. Greenstone Belts and Granite–Greenstone Terranes: Constraints on the Nature of the Archean World. Geoscience Canada 42, 437–484. https://doi.org/10.12789/geocanj.2015.42.081

Vaasjoki, M., Sorjonen-Ward, P., & Lavikainen, S., 1993. U-Pb age determinations and sulfide Pb-Pb characteristics from the late Archean Hattu schist belt, Ilomantsi, eastern Finland. Geological Survey of Finland, Special Paper 17, 103–131.

Vaasjoki, M., Taipale, K. & Tuokko, I., 1999. Radiometric ages and other isotopic data bearing on the evolution of Archaean crust and ores in the Kuhmo-Suomussalmi area, eastern Finland. Bulletin of the Geological Society of Finland 71, 155–176. https://doi.org/10.17741/bgsf/71.1.008

Vanhanen, E., 1990. Tutkimustyöselostus Kuusamossa valtausalueella Vitikkolampi 1, kaiv. rek. n:o 4587 malmitutkimuksista vuosina 1989–1990. Claim relinquishment report 4587/1, 3 p.

Vesanto, J., 2003. Kaivoslain 19 §:n mukainen tutkimustyöselostus Kuusamon Kuparivaaran alueella valtauksilla Kuparivaara 1-3 suoritetuista malmitutkimuksista. Outokumpu Ltd., Archive report, 5 p.

Vrevskii, A. B., 2019. Non-Subduction Petrological Mechanisms for the Growth of the Neoarchean Continental Crust of the Kola–Norwegian Terrane, Fennoscandian Shield: Geological and Isotope-Geochemical Evidence. Petrology 27, 146–170. https://doi.org/10.1134/S0869591119020073